POSITRON SPECTROSCOPY

Paul G. Coleman

Department of Physics
University of Bath
Bath BA2 7AY, U.K.

p.g.coleman@bath.ac.uk

***Encyclopaedia of Applied Spectroscopy,* ed. D.L. Andrews**
(Wiley-VCH, 2009)
pp 115-152

INTRODUCTION

The history of positron annihilation spectroscopy is in many ways an archetypal story of scientific development, from fundamental physics to applications of industrial importance. Predicted by Dirac (1930) and discovered by Anderson (1932), and found to be emitted from artificially-produced isotopes in the same decade (Joliot-Curie and Joliot-Curie, 1934), the use of positrons as a sub-atomic probe of matter was delayed for over a decade by world events.

In 1942 the first fundamental measurement on gamma rays emitted as a result of the annihilation of positrons in solids was performed; Behringer and Montgomery (1942) found that the angle between the two gamma rays which almost always follow annihilation events did not deviate from 180º by more than 15 minutes of arc. Sergio DeBenedetti and his colleagues (1949) were the first to demonstrate that the angle between deviated from 180º by an amount linked to the electron momentum and soon afterwards published their vision of a new spectroscopy of electron momentum distributions – Angular Correlation of Annihilation Radiation (now termed ACAR) (DeBenedetti *et al*., 1950). DeBenedetti was joined in his pioneering work by Page (1956), Stewart (1957) and Berko (1958).

Shearer and Deutsch (1949) pioneered the measurement of the lifetimes of positrons in gases, and it was this technique which led to the experimental discovery (Deutsch, 1951) of the positron-electron bound state, positronium (theoretically considered and named electrum by Mohorovičić (1934) and renamed positronium by Ruark (1945)). Extension of positron lifetime spectroscopy to liquids and solids required faster timing techniques, and these were developed by Bell and Graham (1953) and exploited soon thereafter by Landes *et al.* (1956) and others in the study of structural changes on the atomic scale.

In the 1960s, with the development of more widely-available equipment, the level of activity and sophistication increased in both lifetime and angular correlation spectroscopies – for example, yielding new information on positron slowing down and annihilation in gases (Osmon, 1965) and in metals (Weisberg and Berko, 1967). In this decade experimental problems such as the effect of the radioactive positron source on results, the analysis of data containing multiple lifetime components, and struggles with electronic stability, were still being worked on. In the late 1960s the role of positron trapping in atomic-scale open-volume point defects in solids was first realised (and explained why different laboratories often produced conflicting results for notionally the same sample). Rather than confusing the issue and burying the technique, this realisation gave positron spectroscopy a new lease of life;

positrons are so efficiently trapped by these defects that they soon became a sensitive probe of defect structures and open volumes in a wide variety of solids (e.g. Petersen *et al.*, 1974).

Further advances in instrumentation, coupled with the traditional resourcefulness and inventiveness which has characterised the positron research community over the years, led to the application of Doppler broadening spectroscopy in the 1970s – a high count-rate, lower-resolution measure of electron momentum densities – which quickly grew as its efficacy and scope for application were realised (e.g., Maier *et al.*, 1979). In the same decade ACAR was enhanced by the development of two-dimensional measurements, first by using an array of discrete photon detectors (Mader *et al.*, 1976) and then by using position-sensitive gamma cameras (West *et al.*, 1981) or multiwire proportional chambers (Jeavons *et al.*, 1978).

One of the most significant developments in positron techniques also happened in the early 1970s, with the first useable laboratory-based beams of controllable low energy (eV to keV) (Canter *et al.*, 1972). After a few years' application only in atomic physics (i.e., in positron scattering), these beams were applied to solids and, after a number of groundbreaking fundamental studies of positron-surface interactions (e.g., Mills *et al.*, 1978), have been used widely since the 1980s to study surface and near-surface characteristics, thin films and interfaces (e.g., Triftshäuser and Kögel, 1982). Beam systems – both laboratory and facility-based - are now available delivering positrons with energies controllable between 0.02 eV and ~ MeV at intensities up to almost 10^9 per second.

We shall be focussing on positron spectroscopy of condensed matter; much important fundamental research has been and continues to be performed in atomic physics, but this activity lies outside the scope of this chapter. For an excellent overview of this work the reader is directed to the book by Charlton and Humberston (2001).

1. FUNDAMENTALS

Annihilation of free positrons and positronium

The annihilation of a positron by its antiparticle, the electron, both stationary, can theoretically result in the emission of any number n of gamma rays if n is greater than one. The gamma rays which take away the rest energy $2mc^2$, where m is the mass of each particle and c the speed of light. Zero and single gamma ray emission are forbidden for an isolated positron-electron pair at rest because both energy and momentum have to be conserved; both can theoretically occur in the presence of a third body, however. While the emission two or more gamma photons satisfies both energy and momentum conservation, the probability of n photon emission decreases sharply as n increases (and as the number of vertices on the

corresponding Feynman diagrams (Charlton and Humberston, 2001)). For example, Ore and Powell (1949) calculated that the probability of three-gamma emission is about 370 times less likely than that for two-gamma emission, and the contributions to experimental studies of decays with n greater than three are practically negligible. Consequently, almost all annihilation events involving free (or quasi-free) positrons and electrons result in the emission of two gamma rays of energy mc^2 (511 keV) in opposite directions (to conserve momentum).

If the positron and electron are in the lowest (ground) state of the bound hydrogen-like system called positronium (Ps). Because the reduced mass is half that of the electron in hydrogen, energy levels are half those in hydrogen (e.g., the ground state binding energy is 6.8 eV) and interparticle separations are doubled. Ps annihilation events are governed by a selection rule resulting from CP (charge parity) invariance. The parity of the gamma photons is $(-1)^n$, and for ground-state Ps it is $(-1)^S$, where S is the total spin angular momentum of the Ps atom. If the positron and electron in the Ps have opposing spins (the singlet state, para-Ps or p-Ps) then the total S =0 and consequently n has to be an even number. Conversely, if the positron and electron spins are parallel and S = 1 (the triplet state, ortho-Ps or o-Ps) then n has to be odd. Following the arguments in the previous paragraph, this means that p-Ps decays principally decays into two 511keV antiparallel gamma rays, whereas o-Ps decays into three gamma rays whose total energy is $2mc^2$ or 1022 keV. The distribution of gamma energies from o-Ps decay was calculated by Ore and Powell (1949) and measured by Chang *et al*. (1985), indicating that the majority of o-Ps decays involve the emission of two gamma rays having energies which are a large fraction of mc^2 travelling in roughly opposite directions, with a third low-energy gamma photon emitted at some angle between them. Ore and Powell also computed that the mean lifetime of o-Ps in vacuo is about 140 ns, over 1100 times longer than the 125 ps mean life of p-Ps (Wheeler, 1946).

1.2. The fate of positrons in condensed matter

1.2.1 Positron backscattering A significant fraction of positrons incident upon a target material, whether from a radioactive source or in a monoenergetic beam, are turned around in a few collisions and leave the target with reduced energies. Measurements have shown that there is significant quasi-elastic backscattering and that the angular distribution of backscattered positrons is peaked at angles around the surface normal. Backscatter coefficients η_+ range from a few percent to almost 50%, and depend principally on the incident positron energy and the atomic number of the target material (increasing with both)

(MacKenzie *et al.*, 1973, Coleman *et al.*, 1992). The consequences of backscattering have to be considered in experiments involving the detection of annihilation gamma radiation, where the detection of gamma radiation from the decay of backscattered positrons at sites other than the intended target can corrupt data.

1.2.2 Positron implantation Energetic positrons entering a sample material lose energy via electronic collisions, reaching eV energies in a fraction of a picosecond and then thermalising in a further time period from one to a few picoseconds, depending on the material. This second phase is dominated by phonon interactions, and here the shortest thermalisation times are in metals and small band-gap semiconductors; in insulators and wide band-gap semiconductors several picoseconds may be taken for thermalisation, and in extreme cases positrons may not reach thermal equilibrium before annihilation. This last scenario is also possible for monoenergetic positrons implanted at very low energies (i.e., below about 1keV), which may retain ~ 0.1-1 eV when encountering the sample surface and thus are able to pass through or interact with the surface in ways different from those positrons which have fully thermalised.

We shall hereafter define positron implantation (or penetration) depth as that at which an incident positron reaches thermal equilibrium. Positrons emitted from the nuclei of a radioisotope decaying via positive beta decay penetrate to depths z below the surface of condensed matter targets whose distribution is traditionally given by the implantation profile $P(z) = \alpha \exp(-\alpha z)$, with α (cm) $\approx 16\rho E_m^{-1.4}$ (ρ = density in gcm^{-3}, E_m = maximum beta positron energy in keV). This means that beta positrons can penetrate to depths of ~ 1mm, and are thus used to study the bulk properties of materials. A recent experimental study (Foster *et al.*, 2007) has shown that the exponential model provides a reasonable description of beta positron implantation except at small depths, where it underestimates $P(z)$ by ~ 10%, and very close to the surface, where $P(z)$.should tend to zero rather than its maximum value.

If the incident positrons impinge on a target normally with an energy E, however, their implantation profile has been generally taken to be well described by a Gaussian derivative:

$$P(z,E) = 2(z / z_0^2)\exp(-z^2 / z_0^2) \qquad (1)$$

where the parameter z_0 (in nm) usually taken to be related to E and to the material density ρ (in gcm^{-3}) by the simple expression $(40/\rho)E^{1.6}$. z_0 is 11% larger than the mean implantation depth. While the form for $P(z,E)$ has been shown to be adequate in most cases, the prefactor and the energy exponent have been found to be material-dependent (Baker *et al.*, 1991).

1.2.3 Positron diffusion The diffusive motion undergone by thermalised positrons in condensed matter may be considered principally to involve isotropic elastic scattering from acoustic phonons, and may be described by the diffusion equation because, although the positron is a quantum entity, its wavelength and mean free path (both ~ nm) are small compared with typical total distances travelled before annihilation. The positron diffusivity D_+ is proportional to its mobility η_+, with the constant of proportionality being (kT/e). D_+ varies with temperature as $T^{1/2}$ for scattering off acoustic phonons, as $T^{-3/2}$ for optical phonons, and $T^{3/2}$ for neutral impurities; however, the latter two dependencies are only relevant for certain materials and at very high or very low temperatures. At room temperature D_+ has values of a few cm^2s^{-1} for most metals and semiconductors. The diffusion length of positrons $L_+ = (D_+\tau)^{1/2}$, where τ is the mean lifetime of positrons in a material (having values in the range ~100-200 ps); typical values of $L+$ are ~ 100nm in metals to 270nm in silicon.

1.2.4 Positron trapping Once considered a problem in positron measurements, the propensity for positrons to be trapped efficiently by open-volume point defects – vacancies, vacancy clusters and voids – and at shallow trapping sites such as at a negatively-charged impurity – is now the mainstay of applied positron annihilation spectroscopy. Although the classical picture of positrons being attracted to a region of lower-than average positive charge is commonly used to explain positron trapping, the diffusing positron is a quantum particle and trapping should be considered to be quantum localisation. Positrons provide a unique method for non-destructive characterisation of such defects at concentrations as low as 10^{-7} per atom, saturating at ~ 10^{-4} per atom.

There are two main models describing positron trapping. For small point defects such as vacancies the trapping is *transition-limited* – i.e., dependent upon the probability of trapping once a defect is encountered; this is described by the specific trapping coefficient v, which has typical values in the range 10^{14}-10^{15} s^{-1}. The total trapping rate κ is then vC, where C is the defect concentration per atom. v for semiconductors has a temperature dependence which can be used to identify defect type. The second trapping model is *diffusion-limited* – i.e., determined by the probability of finding the trapping sites which, once found, have a trapping probability of unity. The total trapping rate is then $\kappa = 4\pi RD_+N$, where R (cm) and N (cm^{-3}) are the radius and number density of the defects, respectively, and D_+ is the positron diffusion constant in cm^2s^{-1}.

The charge state of open-volume point defects in semiconductors and insulators can play an important role in positron trapping. The specific trapping rate v is very small for positively-charged defects, whereas neutral sites are effective positron traps and negative charge can increase v by a significant factor. While open-volume defects are deep traps for positrons, shallow trapping can occur around negatively-charged vacancy or impurity defects – this is usually seem at low temperatures and identified by the temperature dependence of the trapping probability (Saarinen *et al.*, 1997).

Thermally-induced detrapping from defects sites can occur, depending on the Boltzmann factor $\exp(-E_b/kT)$, where E_b is the binding energy of the positron in the trap; therefore, for example, for deep traps - i.e., those for which E_b is a few eV - detrapping can be considered negligible.

1.2.5 Positron-surface interactions If a positron encounters the surface of a material sample after implantation it can suffer a variety of fates, all of which have found application in various experimental studies. We shall for the moment assume that the positron has been thermalised before reaching the surface, and not consider at all those backscattered positrons which penetrate the surface without any significant interaction with it.

There are three main channels open to the positron on encountering a surface; (a) trapping in the surface potential well, (b) binding with a surface electron and leaving as Ps, and (c) being re-emitted from the surface by a negative positron work function φ_+. For those materials for which φ_+ is negative, channel (c) is not open.

1.2.5.1 Surface trapping The potential encountered by a positron may be considered for our purposes to be a combination of the attractive image potential - which falls off as the reciprocal of distance from the surface - and the repulsive dipole potential, which falls off significantly more quickly above the surface (i.e., within a few angstroms). The combination of these two potentials thus creates a deep well above the surface in which positrons are efficiently trapped. On an atomically-clean perfect surface the trapped positron can be used as a probe of electronic surface states. If the temperature of the material is increased then the trapped positron can be desorbed, but only via the formation of thermal-energy Ps which supplies its 6.8 eV binding energy; this, however, is an excellent source of low-energy Ps atoms for spectroscopic measurements.

1.2.5.2 Positronium formation For metals and semiconductors the surface is the only site where the electron density is low enough to permit Ps formation. The formation potential for Ps at surfaces, essentially the energy possessed by the emitted Ps atom, is the balance between the sum of the electron and positron work functions – i.e., the energy

required to remove both particles independently from the solid – and the 6.8 eV gained by forming the bound state. In the early days of positron-surface experimentation Ps formation was used as a signature that the positron had diffused back to the surface; however, the probability of forming Ps is critically dependent on surface conditions, which can have a positive or negative influence on measurements. Measurement of the velocity spectra of emitted Ps was also used as a probe of electronic surface states. Of great fundamental importance is the fact that small fractions of the Ps emitted can be in an excited state or as the negative ion Ps^-.

1.2.5.3 Positron re-emission The sum of the correlation and dipole potentials outlined in subsection 1.2.5.1 above (the correlation potential is the asymptotic level of the image potential inside the material) can be positive or negative – i.e., positrons are either attracted or repelled by the surface, depending on their relative magnitudes. The difference between the resultant total potential within a solid and the reference vacuum level far from the surface is the positron work function φ_+. For a number of solids the dipole potential is greater than the correlation potential and φ_+ is negative – i.e., thermalised positrons are emitted from the surface with an energy of ~ φ_+. Negative φ_+ values for metals range from close to zero to ~ 3eV and, like their electron equivalent, are dependent on surface composition and structure. For a perfect surface the emission is normal to the surface, smeared only by thermal effects; for a 'real' surface the emitted positrons may undergo inelastic collisions above the surface which lower their average energy and increase their angular spread; if enough energy is lost in such a collision then the positron may fall into the surface well and be trapped. Thus, there is a correlation between the magnitude of φ_+ and the fraction of positrons re-emitted from a surface.

A small fraction of positrons from a radioactive source incident on a solid with negative φ_+ possess energies low enough (i.e., below ~ 10^1keV) to be thermalised, return to the surface, and subsequently be re-emitted with work function energies. This is the basis of the generation of monoenergetic positron beams, which have been widely used to study surface and near-surface phenomena for the past 25 years.

1.2.5.4 Surface branching ratios The relative probabilities of these three main channels open to the positron are described by the branching ratios ε. For a solid with a positron work function of ~ -1 eV, the three branching ratios are in the approximate ratio of 1:1:1. For surfaces with a positive φ_+ approximately half the positrons form Ps and half fall into the surface trap at room temperature.

1.2.5.5 Non-thermalised positrons If the positrons incident on a surface have energies below about 1keV there is a significant probability that they will return to the surface without being fully thermalised – i.e., with residual energies of several hundred meV. These epithermal positrons interact with the surface with rather different branching ratios; they can more readily overcome surface trapping and leave as positrons with energies above φ_+, and can pick up an electron and form Ps which again leaves with higher energy than that formed by the process outlined in section 1.2.5.2.

On encountering 'real', dirty surfaces – for example, oxide-covered – the branching ratios can be hugely different from those for a clean perfect surface and, in addition, there can be significant, sometimes overwhelming, trapping at surface defects.

We shall next focus on the annihilation of thermal-energy positrons with electrons, and of Ps-like states, in condensed matter. Other aspects of positron and Ps interactions in solids and liquids will be discussed in later sections.

1.2.5 Positron annihilation: observables The cross section σ for annihilation is inversely proportional to positron speed v, but the annihilation rate is proportional to σv. Consequently, although annihilation during positron slowing down is possible, has been observed, and may play a role in some positron experiments (Weber *et al.*, 1999), the overwhelming fraction of annihilation events occur after thermalisation, when positron spend most of their time in diffusive motion.

Although positrons rapidly (i.e., in ~ ps) thermalise in condensed matter, and so can be thought of as quasi-stationary, the electrons which annihilate them are decidedly not. Conduction electrons at the top of the Fermi sea in metals, for example, have several eV energy, and bound electrons can have keV energies. However, most positrons will perish at the hands of the lower-energy conduction or valence electrons, both because of the time of interaction and because of their propensity to spend more time away from the positive ion cores.

If we initially treat the positron and electrons as independent particles (i.e., we ignore mutual interactions) then the probability $\rho(\boldsymbol{p})$ that a pair of gamma rays with total momentum $\boldsymbol{p}$ will result from the annihilation of a positron and an electron is given by

$$\rho(\boldsymbol{p}) = (r_0{}^2 c/8\pi^2) \sum_{i,j} n_i{}^+ n^-{}_j \left| \int\int\int \exp(-i\boldsymbol{p}\boldsymbol{r}) \psi_i{}^+(\boldsymbol{r}) \psi_i{}^-(\boldsymbol{r}) d^3 r \right|^2 \qquad (2)$$

where $n_i{}^+$ and $n_j{}^-$ are the occupancies of the positron and electron states, the former being close to a delta function, and $\psi_i{}^+(\boldsymbol{r})$ and $\psi_j{}^-(\boldsymbol{r})$ are the positron and electron wave functions,

respectively. If we assume that the positron momentum is relatively negligible then $\boldsymbol{p}$ represents the electron momentum at the moment of annihilation.

Direct complete evaluation of the so-called momentum density $\rho(\boldsymbol{p})$ would be possible if one could perform a three-dimensional measurement of the momenta of the annihilation photons. In principle one could achieve this by measuring the *x* and *y* components via the angles between the photons (see Experimental Techniques section) and the *z* component via the Doppler shifts in the measured photon energies. In practice we integrate over the *z* component and record the two-dimensional contour 'map': i.e., $\rho(p_x,p_y) = \int\rho(\boldsymbol{p})\, dp_z$. This is the basis of the experimental technique known by the acronym 2D-ACAR, two-dimensional angular correlation of annihilation radiation.

If instead we integrate over both *x* and *y* components of $\boldsymbol{p}$ then we arrive at the momentum density in the *z* direction, which gives rise to the Doppler broadening of annihilation radiation (DBAR), an extremely useful spectroscopy for following changes or differences in electronic structure: $\rho(p_z) = \iint\rho(\boldsymbol{p})\, dp_x\, dp_y$.

Finally, the total annihilation rate is given by the integral of $\rho(\boldsymbol{p})$ over all three components of $\boldsymbol{p}$: $\lambda = \iiint\rho(\boldsymbol{p})\, dp_x\, dp_y\, dp_z$. Reference to equation (2) shows that λ is proportional to electron density in the vicinity of the annihilated positron. The mean positron lifetime τ is the reciprocal of the annihilation rate λ, and measurement of the various possible lifetime components for positrons in condensed matter forms the basis of positron annihilation lifetime spectroscopy (PALS). The independent particle model leading to equation (1) is inadequate for the calculation of λ; $\rho(\boldsymbol{p})$ has to be multiplied by a positron-electron enhancement factor $\boldsymbol{\varepsilon}$ to take account of the interactions between positron and electrons and between the electrons in the material being studied (Kahana, 1963).

1.2.6 Positronium annihilation Although the quasi-stable bound state positronium (Ps) cannot form in metals or semiconductors, as a result of electron screening (except above the surface – as discussed later), it can exist in insulating solids and liquids.

A small variety of models have been proposed to describe Ps formation in such solids and liquids, and their applicability depends to a large extent on the material under study. The Ore Model (Ore, 1949) considers Ps formation to occur principally in the range of energies from $(E_i - B)$ to E_{ex}, where $E_{ex}$and E_i are the threshold energies for atomic excitation and ionisation, respectively, and B = 6.8 eV is the ground state binding energy of Ps. Above E_{ex} other interaction are assumed to outcompete Ps formation. A second prominent model is the Spur Model, due to Mogensen (1974), in which the positron binds to an electron released in a

spur during the slowing-down process, under conditions of small relative momentum. An extension of this model is to consider the end of the positron track to be a 'blob', rather than a spur (Stepanov and Byakov, 2002). A third, particularly considered with respect to Ps in polymers, involves the formation of Ps in open volumes or holes, the electron being picked up from the surface (Brandt *et al.*, 1960); if the positron is not completely thermalised then the Ps atom may undergo thermalising collisions with hole walls.

There have been many groundbreaking fundamental measurements on Ps over the past fifty years, from precise measurements of vacuum decay rates to measurements on excited states, observations of the negative ion and hydride, and of Ps-Ps interactions en route to a Bose-Einstein Ps condensate (Cassidy and Mills, 2007). In section 3, however, we shall briefly summarise only some of those applications in which Ps decay has been used to characterise condensed matter on the atomic scale, mostly involving the measurement of Ps lifetimes and intensities.

2. EXPERIMENTAL METHODS

Sources of positrons

The two methods for obtaining positrons for use in spectroscopic measurements are (i) radioactive sources and (ii) pair production. The most common radioisotope used in the laboratory is sodium-22 (half-life 2.7 years), with cobalt-58 sometimes used in experiments requiring higher intensities over shorter periods (half-life 71 days). These and other positron-emitting sources are created in reactor cores by nuclear bombardment; a number of steps have been taken towards the in-house creation of strong positron sources using table-top proton and deuteron accelerators to produce short-lived but high-activity radionuclides (Hiros *et al.*, 1997). In-house or facility-based sources are primarily used in the production of intense positron beams, as are positrons created by pair production in a linear accelerator (LINAC). In the latter case bremsstrahlung radiation from pulsed energetic LINAC electrons created electron-positron pairs in a target of high atomic number; the energetic positrons are then moderated to form an intense, often pulsed, positron beam.

Positrons emitted via the positive beta decay of radioactive sources are longitudinally-polarised (ie, spin-polarised in the direction of their emission) as a consequence of parity non-conservation; the weak interaction that mediates beta decay leads to a non-vanishing helicity. This property has been exploited in a number of experiments to study the bulk magnetic properties of materials, principally using ACAR (section 2.3). The principle underlying its application is that positrons are ~1000 times more likely to annihilate an

electron in the opposite spin state. Therefore, if the spin states of some of the electrons in a sample are changed (eg by measuring magnetic and nonmagnetic samples, or by changing the external magnetic field direction), the difference in the experimental data yields information specifically on those electrons and thus the magnetic species.

Lifetime spectroscopy

The first positron spectroscopy to be developed, and still widely used today, involves the measurement of the mean lifetimes of positrons in condensed matter. As introduced in section 1.2.5, the mean lifetime of positrons in condensed matter is related directly to the electron density in the vicinity of the positrons at their moment of annihilation. For example, if positrons are annihilated while trapped in open-volume defects, the average electron density is reduced and the mean lifetime is increased, and there is in general a characteristic lifetime value for every different annihilation state.

In the most general case, positrons can decay from a range of states *s* each with annihilation rates $\lambda(s)$ (λ being the reciprocal of the mean lifetime τ), with the probability of being in state *s* at annihilation being $P(s)$. The resultant lifetime spectrum is

$$I(t) = \int P(s)\exp(-\lambda(s)t)ds \qquad (3)$$

which, if the annihilation proceed via a small, discrete states labelled *i*, reduces to

$$I(t) = \sum_i I_i \exp(-\lambda_i t) \ . \qquad (4)$$

This spectrum can be fitted with standard programs to extract the decay rates (and thus lifetimes) and corresponding intensities, deconvoluting the time resolution of the measuring system and allowing for system-related components such as that associated with positron decay in the source. In practice the number of discrete components which can be reliably obtained from experimental spectra is crucially dependent on the range of values of λ_i and the number of states involved; a maximum *i* value of 3 is typical. A common strategy in many experiments is to use the average positron lifetime $\bar{\tau}$ (or decay rate $\bar{\lambda}$), defined as

$$\bar{\lambda} = \bar{\tau}^{-1} = \int \lambda(s)P(s)ds \ \ or = \sum_i I_i\lambda_i \qquad (5)$$

particularly when it is the change in λ with some external parameter that is important.

2.2.1 Experimental lifetime systems Conventional positron lifetime spectrometers have at their heart a radioactive source, commonly sodium-22 deposited between two thin low-*Z* films, sandwiched between two pieces of the sample to be studied. If the sample is to be cooled or heated during the measurements it may be mounted in a small

evacuated chamber. Sodium-22 provides a 'prompt' 1.28 MeV gamma ray essentially coincident with the emission of the positron, as a result of the de-excitation neon-22; this is detected by a scintillator with a fast response (e.g., barium fluoride or doped plastic) coupled to a photomuliplier. The 511keV annihilation 'death' gamma ray is recorded by a second similar detector assembly, and the fast pulses (rise time ~ 1ns) created are fed into a timing system which records up to about 10^6 time intervals between birth and death gamma rays. Traditionally the timing systems have included single channel analysers to select pulses of appropriate size, a time-to-amplitude converter (usually with a suitable delay line before the 'stop' input, and a multichannel analyser to collect in parallel the entire range of pulse heights (i.e., the entire range of positron lifetimes). In recent years this analogue system has been replaced by a digital equivalent in which every pulse representing a time difference is digitised and stored, allowing post-collection timing optimisation (Fig. 1).

2.3 Angular Correlation of Annihilation Radiation

Although, as discussed in section 1.1 for stationary particles, two-gamma annihilation in the centre of mass frame sees the two photons leaving the site of the annihilation with identical energies (mc^2, 0.511 MeV) in exactly opposite directions (to conserve momentum), in the laboratory frame the momentum of the annihilating pair moving with a velocity v means that the angle between gamma rays – as shown in Fig. 2 – is no longer 180º.

Relativistic transformation from one frame to the other yields expressions for $\tan\theta_1$ and $\tan\theta_2$. Then $\delta\theta \approx \tan(\theta_1-\theta_2)$ which, ignoring terms in $(v/c)^2$, reduces to $(2v/c)\sin\theta_0$. Now if we set $\theta_0 \approx \theta_1 \approx \theta_2 = \theta$, then $\delta\theta \approx 2mv\sin\theta / mc = p_t / mc$, where p_t is the component of momentum of the annihilating pair in a direction transverse to the gamma emission. Measurement of $\delta\theta$ thus directly yields information on p_t. $\delta\theta$ typically ranges up to 20 mrad; in order to achieve the necerssary resolution the gamma detection regions have to be small and spaced many metres from the sample being studied. In one-dimensional studies (1D-ACAR) long thin slits – usually between lead blocks – define the gamma directions; in two-dimensional (2D-ACAR) experiments (Fig. 3) annihilation photons are detected by position-sensitive detectors such as Anger cameras or multiwire ionisation chambers. To effectively eliminate background events positrons are guided from the ~ GBq source to the samples by a strong (~1T) magnetic field over a few cm from a radioisotope source, or by a guiding magnetic field in a low-energy positron beam system. About 2 x10^8 coincident annihilation events are typically recorded. Samples are commonly mounted in a small vacuum chamber on a cold finger to enable measurement at temperatures down to ~10^1 K, and can be fixed at

different crystalline orientations. Anger cameras have spatial resolution of 2-3 mm, so that if mounted at ~15m on either side of the sample provide angular resolution of ~ 0.2 mrad. Somewhat better resolution is possible with multiwire proportional counters. These high-resolution capabilities have found their place in the measurement of occupied electron states, and thus the Fermi Surfaces of a number of simple and complex solids (see section 3.5 for examples). The Lock-Crisp-West (LCW) procedure (Lock *et al*, 1973) folds the momentum density back into the first Brillouin zone which then gives a distribution which directly indicates the occupancy of states across the projected zone. (The Fermi surface is defined by whether a particular state is occupied or not for each band, and these occupancy breaks are revealed directly by 2D-ACAR.) The full three-dimensional Fermi surface can be reconstructed tomographically from an appropriate number of two-dimensional projections along different crystallographic orientations.

2.4 Doppler broadening of Annihilation Radiation

The component of the momentum p_p of an annihilating positron-electron pair in the direction of emission of the annihilation gamma photon gives rise to a Doppler shift in the photon energy of $\pm cp_p/2$. For example, if p_p arises almost wholly from an electron moving close to the Fermi level with a kinetic energy of 5eV, $cp/2$ = 1130 eV. This is of the same order as the energy resolution of a high-purity germanium detector. Because the electrons can have a component of momentum toward or away from the detector at the moment of annihilation, Doppler broadening around mc^2 (511keV) is measured. Changes in the annihilation linewidth from a fraction of 1% to a few % are typically measured and, although the technique provides a measure of the average electron momentum which is of considerably lower resolution than ACAR, its high signal rates and relative simplicity has found wide application in the study of defects and phase changes in materials. This is referred to as Doppler Broadening Spectroscopy (DBS) or Doppler Broadening of Annihilation Radiation (DBAR).

A typical system for DBAR is sketched in Fig. 4. The Ge crystal is cooled by liquid nitrogen or by an electrical cooler to eliminate effectively thermal noise. A preamplifier is routinely mounted inside the cooled detector head. The optional biased amplifier allows expansion of the photopeak into a larger number of channels on the multichannel analyser (MCA). Because small drifts can broaden the spectrum stabilisation is necessary, and this is achieved by temperature control and by using a digital stabiliser set to a nearby reference line

- e.g., the ^{7}Be 478 keV gamma line. Digital systems have been developed which house all the elements shown in Fig.4.

Samples for DBAR are typically mounted in an evacuated chamber to avoid sample contamination on heating or cooling, and data contamination by annihilation signals in air; such mounting also enables temperature control. For traditional bulk measurements using a radioactive source two pieces of the sample material sandwich a source held in low-*Z* films, and correction has to be made for annihilations in the source itself; if the sample is at the target end of a positron beam system then no source correction is necessary.

Resultant 'photopeak' spectra corresponding to the annihilation gamma line are quasi-gaussian in shape; entirely free (i.e., conduction) electrons would lead to a parabolic peak, and core electrons to a number of increasingly small 'side' peaks; the sum of these contributions has a gaussian, or multigaussian, appearance. The central part of the annihilation line thus preferentially contains contributions from the lower-momentum conduction and/or valence electrons, while the wings contain contributions from annihilation with core electrons. Analysis routines have been developed which take account of the detailed shape of the peak, with a view to maximising the amount of information obtained in Doppler broadening experiment, although it is more common to use the raw data to track *changes* in lineshape parameters under changing experimental conditions.

We shall later see that, by decreasing background significantly, detailed analysis of the peak shape can exploit the technique's sensitivity to the elemental environment. However, we shall first consider the standard method for describing the Doppler-broadened linewidth—i.e. the use of simple lineshape parameters. The most common parameters used are called *S* and *W* – the sharpness and wing parameter, respectively - which are defined in Fig. 5. Three regions of the peak – here A (central),and C and E (the two wings) - are chosen, symmetrically about its centroid. The limits of these regions are chosen such that the central and total wing fractions of the peak area – which are called the *S* and *W* parameters - are ~ 0.5 and ~ 0.1- 0.2, respectively. Background is first subtracted if deemed necessary. Following our argument above, *S* and *W* should reflect principally changes in the momentum density of lower- and higher-momentum electrons, respectively. For example, positron annihilation in open volume defects typically leads to an increase in *S* and a decrease in *W*.

Neither *S* nor *W* have absolute values, as it is their dependence on external parameters that is commonly of interest. However, it is common to express the parameters normalised to bulk values – i.e., S/S_{bulk} and W/W_{bulk}, where the denominators are the parameters associated with the defect-free bulk material being studied, measured with the same apparatus. The

choice of which parameter to use (S and W are not the only choices) , and the limits of regions defining the parameters, are system-dependent.

If S_f and W_f are the S and W parameter characteristic of free positrons, then we can define a new parameter R, $= |(S - S_f)/(W - W_f)|$, which depends only on the nature of the defect, and not on its concentration. If R is found to be constant then this points to the existence of only one kind of defect (Mantl and Triftshäuser, 1978).

2.4.1 Two-detector DBAR This technique was proposed many years ago by Lynn *et al.* (1977) but has been reintroduced and developed in the past decade. If a sample is viewed by a second gamma photon detector, and pulses from the two detectors (in coincidence) are fed into the inputs of a two-dimensional multichannel analyser array, a photopeak results which not only has vastly reduced background (i.e., by two or more orders of magnitude), but the resolution is decreased by a factor of $\sqrt{2}$. Example data for such a system are shown in Fig. 6. This method enables one to study annihilations with core electrons and, in the case of recent studies with positron beams, identify the chemical environment in which the positron decays. The measurement typically involves the accumulation of single annihilation line spectra of high statistical precision whose shape is analysed carefully and compared with calculations.

2.4.2 Age-momentum correlation (AMOC) Simultaneous measurement of positron lifetime and the momentum of the annihilating pair (i.e., PALS + DBAR) can give information on thermalisation and transitions between positron states (and hence on chemical reactions of positrons or Ps). The most recent version uses an MeV positron beam (Siegle *et al.*, 1997).

2.5 Positron beams

Positron beams offer two major advantages over traditional positron systems: (a) the control of incident positron energy, and thus average implantation deths from the surface to depths of ~ μm, and (b) the separation of the thermalisation of positrons implanted into a material from their eventual annihilation in another. This has led to new applications in surface, near-surface, interface and thin film studies.

The re-emission of work-function-energy positrons from a solid surface was outlined in section 1.2.5.3. In the case of simple metals the fraction of implanted positrons reaching an exit surface is optimised if the if the moderator metal contains very few non-equilibrium defects. This means annealing, preferably *in situ*, to as high a temperature as possible (say ~$0.8T_m$) in as low an ambient pressure as possible (e.g. ~10^{-6} Pa or less). Because of its high

positron work function ($\varphi_+ \sim 2.7$ eV), however, tungsten operates well as a positron moderator after greatly-varying preparation procedures. The same is not true, for example, with nickel or copper – whose $\varphi_+ \leq 1$ eV - for which careful surface cleaning and maintenance is required.

Many moderator geometries have been used; the simplest and most common is the mesh, which has quasi-transmission geometry. Moderator efficiencies are commonly in the $10^{-4} - 10^{-3}$ range. Choice of moderator material and geometry is governed by the application of the positron beam – for example, for many applications the priority is simply to maximise moderator efficiency, whereas for others a well-collimated parallel beam requires a planar low-ϕ_+ surface cooled to minimise thermal smearing.

The highest moderation efficiencies (above 10^{-3}) recorded are for solid rare gases, in which positrons do not fully thermalise and have a long effective diffusion length, which can be condensed directly on to the radioactive source capsule.

It has long been recognised that moderation efficiency could be greatly enhanced by drifting a larger fraction of thermalised positrons to the exit surface by an internal electric field, but there has been little practical progress to date on the realisation of such field-assisted moderators.

2.5.1 Laboratory-based beams A standard slow positron beam system (Fig. 7) comprises a flight tube pumped to high or ultrahigh vacuum; positrons ($\sim 10^5$ s^{-1} from a ~4 GBq primary source) are transported in an axial magnetic field, sometimes with focussing elements. Unmoderated (beta) positrons may be filtered from the beam by a curved section or an ExB velocity filter and the positrons are accelerated to the final desired energy either by raising the source of the system to a positive potential or by holding the sample at a negative potential. Beam positioning may be fine-tuned by using a pair of trim coils. Annihilation radiation from the sample target passes through a thin foil window to the Ge detector for DBAR measurements; detection of radiation from the source is minimised by shielding and by making the system a few metres in length. These considerations are relatively unimportant if the system is to be used for particle spectroscopies – see Fig. 8 - especially if electrostatic transport and focusing is in used (Roach *et al.,* 1995).

Brightness enhancement is achieved in positron beams by repeated focusing and remoderation (see Fig. 9). Although remoderation losses may be 70%, the beam area can decrease by a factor of ~ 50 at each stage; hence beam intensity per unit area can increase after n stages by a factor 15^n.

2.5.2 High-intensity positron beams Standard laboratory beam intensities up to ~10^6 controllable-energy positrons per second are currently available, and a great range of experiments have been performed with such beams. However, to extend the capabilities and realise the full potential of positrons as a spectroscopic tool, more intense beams are essential, for many studies in which the probability of an outcome is very small; for example, the combination of controlled implantation with 2D-ACAR, many surface spectroscopies where rapid measurements are required, and the study of many-positron systems.

Facility-based systems – both reactor and LINAC-based - are still a main focus for intense positron beam generation, but in recent years there has been a movement towards the use of small-scale laboratory-based accelerator systems to produce short-lived but intense positron sources. In the case of LINACs (section 2.1) the beam is pulsed (section 2.5.3); this property can be exploited in applications where timing is an advantage. In laboratories in reactor complexes an intense positron beam is guided far from the core and possibly subjected to remoderation, focussing, and bunching for timing applications. The production of positrons in reactor cores is not solely via the creation of intense radioactive sources, but can also proceed via pair production by energetic photons; steps have to be taken to overcome radiation damage problems in the reactor core. Several intense beam systems are in operation or are currently being developed across the world.

2.5.3 Beam bunching LINAC beam pulses are of widths from several ns to μs; if subnanosecond timing resolution is required the positrons must be put through a buncher. Several buncher designs have been put into practice; the first, by Mills (Mills, 1980) - used magnetic mirrors. Later bunchers use RF chopping and bunching techniques—for example, the system at Munich (Bauer *et al.*, 1987) which can now achieve a timing resolution below 200ps.

2.5.4 Positron microbeams Beams of ~ μm dimensions have been created in the laboratory (Fig. 10) for (a) optimum areal brightness and (b) position-sensitive annihilation spectroscopy. (a) is important in positron re-emission microscopy systems in which the microscope optics requires a small but very bright spot – the contrast mechanism in positron re-emission microscopy (PRM) is based on the position dependence of the probability of positron re-emission from a surface. (b) is required for the building of μm-resolution annihilation maps of near-surface structural defects by beam rastering, as has been achieved in Munich (David *et al.*, 2001).

2.5.5 Polarized positron beams It was discovered in 1979 that the depolarisation resulting from moderation of the beta positrons by a moderator, the basis of the creation of controllable-energy positron beams, is negligible (Zitzewitz *et al.*, 1979). Highly-polarised positron beams can in principle probe, non-destructively, and with a degree of depth sensitivity, spin-polarised electrons in thin films or in modified near-surface regions (to depths of a few μm) of materials. Standard laboratory-based beams have to be adapted in two main ways; (a) the high-Z backing behind the radioactive source has to be replaced by a low-Z material to minimise backscattering, and (b) the source has to be positioned further away from the moderator so to select primary positrons emitted into a small forward cone (both (a) and (b) result in loss of beam intensity). The spin polarisation of a positron beam is given by

$$P = (v/2c)(1+\cos\alpha) \qquad (6)$$

where v is the emission velocity, c the speed of light, and α the half-angle of the cone of acceptance of beta positrons at the moderator. (v/c is called the helicity.) For positrons emitted in a cone of half-angle 30º from the commonly-used source ^{22}Na, $P \sim 70\%$.

There has been little exploitation of this property of positron beams, apart from an early experiment which demonstrated their capacity to probe surface magnetism (Gidley *et al.*, 1982). The principle of the measurements is based in the comparison of DBAR or annihilation line profile data for differently-polarised samples.

2.5.5 MeV positron beams High-energy (~MeV) monoenergetic positron beams have been built and used in recent years. MV accelerators used in this work have been of Pelletron or Van de Graaff type. Source-free lifetime measurements in a wide range of materials, beam-based AMOC, and novel annihilation spectroscopies are possible with such systems – for example, positron channelling and in-flight annihilation studies, and bulk annihilation measurements which are free of problems associated with the presence of a positron source.

2.5.6 Trap-based beams Surko and co-workers have developed a source of very low energy positrons with extremely low energy (~ meV) energy spread (Gilbert *et al.*, 1997) which has found wide and important applications, particularly but not solely in atomic and molecular physics. The principle of their system is that positrons are extracted from a plasma of thermalised positrons stored in a Penning-type trap (Fig. 11). The resulting beam can be dc or pulsed. Similar trap-based positron beams have been successfully employed in the antihydrogen work at CERN and other laboratories prosecuting new fundamental research.

2.5.7 Positron beam-based spectroscopies The traditional spectroscopies (PALS, ACAR and DBAR) have all been performed with positron beams, giving the extra information on depth dependence and the ability to probe depths up to ~ μm from a sample surface. The acronyms for such spectroscopies may be constructed by inserting 'VE' (for variable-energy) before those for the bulk spectroscopies. In all these cases codes such as VEPFIT (van Veen *etr al.*, 1990) and POSTRAP (Aers *et al.*, 1995) are commonly employed to separate and identify contributions to the measured parameters from annihilation events over a range of depths from different states such as vacancy-type defects, bulk material, interface regions and the sample surface. The diffusion equation is solved and – for example, with VEPFIT – the positron parameter (like the lineshape parameter S) and associated effective positron diffusion length characteristic of each chosen layer below the surface is evaluated to achieve best fit to the experimental data. In some cases – e.g., where there is one type of trapping centre of concentration C_D per atom – the fitted parameter and diffusion length are linked, and self-consistency can be checked. As an example, let S be the fitted lineshape parameter for a particular layer beneath a surface (i.e. between two given or fitted depths). Then $C_D = (\lambda/v)(S\text{-}1)/(S_D\text{-}S)$, where λ and v were defined in section 1.2.4. Additionally C_D can also be written in terms of the effective diffusion length L as $(\lambda/v)[(L_+/L)^2\text{-}1]$, where L_+ is the positron diffusion length in the undefected 'perfect' material. Equating these two expressions one arrives at $L^2 = L_+^2[(S\text{-}S_D)/(1\text{-}S_D)]$.

The depth resolution of VEPAS techniques degrades as the mean positron implantation depth increases; the width of $P(z,E)$ (section 1.2.2) is comparable to the mean depth. This means that, although resolutions of ~ 50nm is possible for near-surface characterisation, one relies on fitting codes or known sample parameters (like film or layer thicknesses) to model depth profiles at deeper depths. The only method for maintaining depth resolutions similar to that near the surface is to employ an etch-and-measure technique, removing sequentially thin layers of material and probing the progressively-revealed new surface regions with low-energy positrons. The problem with very near-surface layers or thin films is the propensity for positrons to diffuse out of them, either to the surface or to nearby material, and careful fitting and/or data interpretation is required; this problem is less severe for thin layers with a very short positron diffusion length (e.g. oxides). The effects of internal electric fields must also be considered. Finally, the influence of non-thermalised positron interactions at low incident positron energies E has to be recognised, and for this reason data for E below ~ 1keV is often ignored.

An alternative to the use of fitting codes is the identification of different annihilation sites (e.g., layers) using the graphical method of plotting *S* vs *W* parameters for each incident energy *E*. An example will be shown in section 3.4. If there are two possible annihilation states with their characteristic *S* and *W* values – such as the sample surface (subscript *S*) and bulk (subscript *B*)– then an *S*-*W* plot will be a straight line joining the two points (S_S,W_S) and (S_B,W_B) on the graph. Consider a third state, corresponding say to a defected layer with characteristic $S = S_D$ and $W = W_D$ (note that these are average *layer* values, not those specific to a particular defect): if there are energies *E* for which effectively all the positrons are annihilated in this layer then the *S*-*W* plot will have two straight lines joining (S_S,W_S), (S_B,W_B) and (S_D,W_D). Importantly, however, even if only a *fraction* of the positrons decay in the layer at any energy *E*, extrapolation of lines on the resulting *S*-*W* plot will still identify the point (S_D,W_D) – just as a fitting code such as VEPFIT does. *S*-*W* are thus a powerful visual tool for identifying different annihilation sites.

2.5.7.1 Positron surface spectroscopies Notwithstanding the fact that full realisation of positron beams as a surface probe via positron diffraction, re-emission or annihilation will not come until intense positron beams are widely available, much progress has been made over the past 25 years. We shall not here mention positron microscopy, which was visited in section 2.5.4.

Low-energy positron diffraction (LEPD) was pioneered by Canter and co-workers at Brandeis University in 1980 (Rosenberg *et al.*, 1980) and developed by the same group over the next two decades to a level at which they could demonstrate that LEPD can be used to achieve qualitatively and quantitatively better agreement between experimental and theoretical I-V profiles (diffracted beam intensity vs. energy), leading to significantly more reliable determinations of the surface structure than is possible using the traditional electron equivalent, LEED. This improved performance is for the following reasons: (i) the phase shifts for positron scattering are less sensitive to atomic number than those for electrons, so that LEPD is more sensitive to structural parameters in multicomponent systems: (ii) the inelastic mean free path, which plays an important role in the determination of probe depth, is smaller for positrons than for electrons, and so LEPD has a greater surface sensitivity than LEED: (iii) uncertainties in the positron-electron correlation term used in LEPD calculations are less important than the equivalent electron-electron uncertainties in LEED: (iv) positrons are decelerated as they approach ion cores and so relativistic effects such as spin-orbit coupling are reduced for positron scattering from surfaces containing high-*Z* atoms, and LEPD I-V profiles are only weakly spin-dependent when compared to LEED: and (v) as a

result of the absence of spin-exchange repulsion positrons interact more weakly with interstitial valence electrons and so the muffin-tin model works better for LEPD than for LEED for covalently-bonded semiconductors.

Reflection high-energy positron diffraction (RHEPD) has been demonstrated by Kawasuso and Okada (1998), A 20 keV, highly parallel positron beam is incident upon the surface being studied at glancing (< 5°) angles. The most important difference between RHEPD and its electron equivalent, RHEED, is that the high-energy positrons can undergo total reflection from the surface because of the positive crystal potential, and are thus very sensitive to the presence of adsorbate atoms, topological irregularities, and lattice vibrations in the topmost surface layer.

Positronium reflection from LiF was observed by Weber *et al*. in 1988, to date the only report of experimental work in this area.

Positron-annihilation induced Auger electron spectroscopy (PAES) has been developed by Weiss and co-workers since the late 1980's (Weiss *et al*, 1988). Auger electron emission in PAES results from annihilation of a surface core electron by a positron implanted with very low (~ 10^1 eV) energy, rather than from impact ionisation as in its electron equivalent (EAES). The two major advantages of PAES over EAES are the elimination of secondary electron background and the extremely high surface sensitivity. Ohdaira and co-workers have developed a time-of-flight PAES system at ETL, Japan (Ohdaira *et al.*, 1997).

Positronium emission spectroscopies can provide information on electronic surface states; for example, assuming that Ps formation is a sudden process, a measurement of the Ps velocity distribution should yield information on the electronic density of states, although there remains a discrepancy between theory and experiment at low Ps energies.

2D-ACAR was first used in the mid-1980's to attempt to observe directly the positronic surface state; the observed symmetrical momentum distribution may have instead been a signature of localised surface trapping (Lynn *et al.*, 1985). 2D-ACAR was, however, successfully used to study Ps momentum distributions, and showed sensitivity to electronic structure (Chen *et al.*, 1987).

Re-emitted positron spectroscopy measures the energy spectra of positrons re-emitted from a film-covered surface as a function of overlayer thickness (Gidley 1989, Ociepa *et al.*, 1990) which has been shown to be an excellent probe of any processes that affect the sum of the positron and electron bulk chemical potential, including alloying of the overlayer film.

Positronium formation spectroscopy - i.e., monitoring variations in Ps yield (both in magnitude and dependence on incident positron energy) or in the Ps contribution to 2D-ACAR spectra, is an extremely sensitive tool for monitoring oxide growth on metals and semiconductors.

Future developments in positron surface studies may include *positron-induced ion desorption*, *surface barrier potential measurements* via very low energy (~ eV) positron reflection, glancing-angle RHEPD, and the dependence of the Ps formation probability on incident positron energy (coupled with LEED -for the surface atomic configuration - and angle-resolved ultraviolet photoemission spectroscopy, for information on electronic states). Similar measurements can give information on the atomic positions of the adatoms, even if these are hydrogen (in contrast to the conventional angle-resolved photoemission). In *inverse Ps formation spectroscopy* a beam of Ps atoms bombards a surface, the electron is given up to an unfilled state and the positron takes away information on that state; this spectroscopy should be more sensitive than existing probes.

The advance of positron surface science, however, awaits more widespread availability of intense positron beams. Examples of developments which may flow from such availability include *positron holography*, proposed as intrinsically more suitable than electron holography because of the positron's weak scattering and large damping in solids: *polarised PAES*, in which a highly polarised incident beam of positrons create polarised core holes to enable novel studies of magnetic surfaces: *re-emitted positron energy loss spectroscopy*, *Ps diffraction*, and *inverse Ps formation*.

3. EXAMPLES OF RESEARCH USING POSITRON SPECTROSCOPIES

The following examples are designed to provide an overview rather than a detailed summary of every important result obtained using PAS and VEPAS techniques. A relatively small number of examples will thus be selected to demonstrate the applicability of the various techniques.

3.1 Vacancy-type defects

The propensity for diffusing positrons to trap in open-volume point defects has been the basis of one of the major applications of positron spectroscopy.

The measurement of formation enthalpies H_V^F for thermally-generated equilibrium defects has long been a staple of PAS in bulk solids. Both DBAR and PALS have been used for such studies. Fig. 12 shows a recent measurement of mean positron lifetime τ_m in the alloy

Cu_3Sn; the rise in τ_m above 433K indicates the formation of vacancy traps. The positron trapping rate κ is deduced from the measured positron parameters (either lineshape or mean lifetime – let us call them P here) normalised to the bulk defect-free value P_b (so that $P_b = 1$) as

$$\kappa = (P\text{-}1)/(P_d\text{-}P) \tag{7}$$

where P_d is the parameter associated with the defect (in Fig. 12, the high-temperature asymptotic value). The slope of the Arrhenius plot of $\ln\kappa$ vs 1/T then yields the vacancy formation enthalpy H_V^F. In this example the value of H_V^F was similar to that measured for Cu, suggesting that the vacancies are being formed on Cu sites.

Non-equilibrium vacancy defects, such as those induced by strain or implantation, have also been widely studied by PAS. Fig. 13 shows raw VEDBAR data showing a typical response to defects (principally divacancies) produced by 2MeV Si^+ ion implantation into Si for a range of ion doses from 10^{11}-10^{15} cm^{-2} (Coleman *et al.*, 2002). Observations from this and other measurements for MeV ions of widely different masses led to the universal expression for divacancy concentrations at ~ half ion range

$$C_D = (2.79\text{x}10^{10})\ \phi_A{}^{0.63} \quad cm^{-3} \tag{8}$$

where ϕ_A is the ion dose corrected by a multiplying factor equal to the vacancy/ion/Å figure provided by the widely-used simulation code SRIM (www.srim.org).

PAS can give information about dislocations – both in bulk materials and in thin films (e.g., relaxed SiGe) – primarily because it is thought that vacancies exist in kinmks along the dislocation line, and diffusing positrons are thus trapped by them.

3.2 Structural changes

PAS has been, and continues to be, exploited in the study of structural changes associated with phase transitions, precipitation, deformation, etc., induced thermally (including ageing at room temperature) or mechanically. For example, monitoring the *S* parameter as the steel Fe-Mn-Si-Cr-Ni is deformed (Mostafa *et al.*, 2007) shows no response below a few percent strain, as the macroscopic deformation associated with reorientation of martensite plates does not create micro-defects which trap positrons. Above ~5% strain *S* increases as vacancy sites are created, some perhaps along dislocations, until at ~ 16% strain and above the response starts to saturate as all positrons become trapped; this behaviour is also seen in CuZnAl shape memory alloys. The nonlinearity of the corresponding *S*-*W* plot (see section 2.5.7) suggests that there is a variety of defect types created, and/or that the alloy undergoes a γ-ε phase transition during deformation (as seen in microscope images).

3.3 Nanoparticles

An important recent advance in PAS has resulted from the observation that positrons can act as 'magic bullets' in the study of embedded nanoparticles, either residing in the open volume around the particles or being preferentially attracted to them via their greater positron affinity. In both cases the positrons are much more sensitive to the nanoparticles than would be expected from geometrical arguments alone. An example of this, which in addition illustrates the use of coincidence DBAR to gain chemical information on the atomic environment of the annihilated positrons, is shown in Fig. 14 (Nagai *et al.*, 2000). The spectra shown are ratios of the outer wing parts of the measured annihilation line to that for Fe. Positrons are shown to be annihilated preferentially by Cu electrons as Cu nanoparticles form in a dilute (1%) alloy of Cu in Fe, by virtue of the 1eV-deep well created by the relative positron affinities of Cu and Fe.

3.4 Interfaces

Positrons are generally significantly more sensitive to interface states than geometric models would suggest, as they are commonly trapped there during diffusion. An example of VEPAS response to interfaces is shown in Fig. 15, which also demonstrates the usefulness of the graphical parameter-parameter method; here two *W* parameters, rather than the more usual *S* and *W*, have been plotted (Coleman *et al.*, 2007).

3.5 Fermi surfaces

Knowledge of the details of Fermi surfaces can aid understanding of material properties, and 2D-ACAR represents a major tool for probing such surfaces. An example is a study of a rare-earth nickel borocarbide, which exhibit competing or coexisting antiferromagnetism and superconductivity. Dugdale *et al*. (1999) found evidence supporting this from the nesting behaviour found in a particular sheet of the Fermi surface for $LuNi_2B_2C$ (Fig. 16).

3.6 Nanoporous materials and open volumes in polymers

The application of positronium and positron lifetime measurement has long been used as a probe of open volume in polymers, often used in conjunction with other experimental techniques such as differential scanning calorimetry and ionic conductivity measurements. An example of a recent application was a study of polyethylene glycol dimethacrylate (Fig. 17), where PALS was performed for temperatures in the range 100 - 370 K (Bamford *et al.*, 2001). These measurements allow the evaluation of the glass transition temperature, coefficients of expansion of the hole volume, fractional free volume and hole number density.

There has been much activity in recent years in the area of pore size measurement and distribution in thin low-*k* dielectric layers grown for nanoelectronics applications. The basis of these measurements is that Ps can form in nm-sized pores, and its lifetime is linked to pore size. It is also possible to measure lineshape parameters and the ratio of three-gamma (o-Ps) to two-gamma decay events, both sensitive to the decay of Ps, to obtain some measure of the size, number density and interconnectivity of the pores. These methods can be applied to films of thickness ~ μm, and can provide some depth sensitivity, if linked to a positron beam system. Because Ps lifetimes can be ~ ns, timed beam systems can be constructed with relatively long timing resolutions, such as that of Gidley and coworkers (2000), Fig. 18, who use the detection of secondary electrons to tag incident positrons. Interconnectivity can result in Ps escape as a long-lived naturally-decaying entity in the vacuum space above the sample.

3.7 Surfaces

Although there have been in recent years several new initiatives in positron-surface studies, and activity in the ultra-thin-film and polymer coating field which could be considered to be surface science, we shall focus here on the two spectroscopies with the longest history and the most impressive results to date – i.e., positron-annihilation-induced Auger electron spectroscopy (PAES) and low-energy positron diffraction (LEPD).

A recent example of the power of PAES, illustrating the advantages outlined in section 2.5.7.1, involved the study of Se passivation layers on the Si(001) surface by time-of-flight PAES (Zhu *et al.*, 2005). The Se monolayer was found to be stable after days of air exposure, the physisorbed oxygen on the passivated surface being desorbed below 400°C. The Se passivation layer desorbs from the Si(001) surface above 800°C in UHV (Fig. 19).

In the clearest demonstration of the advantages of LEPD over LEED for the evaluation of the surface structure of some materials – specifically here compound semiconductors - Chen *et al.* (1993) showed that the multiple-scattering theory fits LEPD data better than LEED and hence yields structural parameters with smaller uncertainties, and suggested that the differences between LEPD and LEED results were real (see Fig. 20).

3.8 Positron microscopy

The Brandeis positron re-emission microscope used brightness enhancement to obtain a bright microbeam of ~ 5 μm diameter (FWHM) and ~ 10^6 positrons sec^{-1}. The microscope was able to image defect structures on the surface of a thin Ni(100) film with a spatial resolution of 300 ± 10nm (Brandes *et al.*, 1988) – see Fig. 21. Improved resolution should be possible with the application of intense positron beams. More recently there has been work

aimed at further exploitation of positron re-emission microscopy in Japan, and in Munich a ~ μm pulsed beam (David *et al.*, 2001) was rastered across a surface exhibiting a fatigue crack on the micron scale, creating the two-dimensional positron lifetime image shown in Fig. 22 which showed the presence of vacancy defects around the crack invisible to standard microscopic methods (Egger *et al.*, 2002)..

3.9 Positron and positronium chemistry

Some current areas of activity in positron and Ps chemistry were mentioned separately in section 3.5. The formation of Ps in liquids, its enhancement and inhibition, electron and positron scavenging reactions, the formation of positron and Ps bound states, Ps trapping in 'bubbles' in liquids, Ps oxidation and spin conversion, have been studied experimentally using PALS, DBS and ACAR spectroscopies as well as AMOC (section 2.4.2). Rate constants for Ps reactions have been deduced; because Ps is a light particle its diffusion time has to be taken into account. Further details on the chemical reactions of positrons and Ps can be found in the book edited by Jean *et al.* (see 'Further Reading').

ACKNOWLEDGEMENTS

The author is grateful for the support of the Engineering and Physical Sciences Research Council, UK, over many years, and currently under grant EP/F029829/1. He also acknowledges the guidance he obtained from the earlier contribution to this Encyclopedia of Csaba Szeles and Kelvin Lynn.

GLOSSARY

Angular correlation: The angular distribution of two annihilation gamma photons about 180º, directly related to the momentum distribution of the annihilating pair (and hence, in condensed matter, essentially the electron momentum density).

Annihilation: The decay of a positron-electron pair, with the emission of energy in the form of gamma radiation; for free particles, two photons are most commonly emitted.

Doppler broadening: The broadening of the annihilation gamma line due to the non-zero momentum of an annihilating positron-electron pair.

Lifetime: The mean life of a positron in a material.

Positron: The antiparticle of the electron.

Positronium (Ps): The quasi-stable positron-electron bound state, existing as ortho-Ps (spin 1) or para-Ps (spin 0), decaying naturally with the emission principally of three or two photons, respectively.

Specific trapping coefficient: The probability of positron trapping by a particular type of defect per second per defect site. The product of this coefficient and the defect concentration (per atom) gives the trapping rate.

Trapping: The localisation of positrons (and sometimes Ps) in defects sites; vacancy-type defects are deep traps, negatively-charged impurities are shallow traps.

Works cited

Aers, G.C., Marshall, P.A., Leung, T.C., Goldberg, R.D. (1995), *Appl. Surf. Sci*. **85**, 196-209.

Anderson, C.D. (1932), *Science* **76**, 238-239.

Baker J.A., Chilton N.B., Jensen, K.O, Walker, A.B., Coleman, P.G. (1991), *Appl. Phys. Lett*.**59**, 2962-2964.

Bamford D., Dlubek, G., Reiche, A., Alam, M.A., Meyer, W., Galvosas, P., Rittig, F. (2001), *J. Chem. Phys.* **115**, 7260-7270.

Bauer, W., Maier, K., Major, J., Schaefer, H.-E., Seeger, A., Carstanjen, H.-D., Decker, W., Diehl, J., Stoll, H. (1987), *Appl. Phys. A* **43**, 261-267.

Behringer, R., Montgomery, C.G. (1942), *Phys. Rev*. **61**, 222-224.

Bell, R.E. and Graham, R.L. (1953), *Phys. Rev*. **90**, 644-654.

Berko, S., Plaskett, J.S. (1958), *Phys. Rev.* **112**, 1877-1887.

Brandes, G.R., Canter, K.F., Mills, A.P. (1988), *Phys. Rev. Lett*. **61**, 492-495.

Brandt, W., Berko, S., Walker, W.W. (1960), *Phys. Rev.* **112**, 1289-1295.

Canter, K.F., Coleman, P.G., Griffith, T.C., Heyland, G.R. (1972), *J. Phys. B* **5**, L167-169.

Canter, K.F., Dharmavaram, V., Smirnov, A.G., Wesley, S.A., Wong, K.A., Xie, R., Brandes, G.R., Mills, A.P., Jr. (1994), *Slow Positron Techniques for Solids and Surfaces* (Ottewitte, E., Weiss, A.H., Eds.), New York: AIP Conf. Series 303, p. 385.

Cassidy, D.B., Mills, A.P., Jr. (2007), *Nature* **449**, 195-197.

Chang, T.-B., Tang, X.-W., Li, Y.-Q. (1985), *Phys. Lett.* B**157**, 357-360.

Chen, D.M., Berko, S., Canter, K.F., Lynn, K.G., Mills, A.P. Jr., Roellig, L.O., Sferlazzo, P. (1987) *Phys. Rev. Lett.* **58** 921-924.

Chen, X.M., Canter, K.F., Duke, C.B., Paton, A., Lessor, D.L., Ford, W.K. (1993), *Phys. Rev. B* **48**, 2400-2411.

Coleman, P.G., Albrecht, L., Walker, A.B., Jensen, K.O. (1992) *J. Phys. Condens. Matter* **4**, 10311-10322.

Coleman, P.G., Burrows, C.P., Knights, A.P. (2002), *Appl. Phys. Lett.* **80**, 947-949.

Coleman P.G., Burrows C.P., Mahapatra R., Wright N.G. (2007), *J. Appl. Phys.* **102**, 014106-1-4.

David, A., Kögel, G., Sperr, P., Triftshäuser, W. (2001), *Phys. Rev. Lett.* **87**, 067402-1-4.

DeBenedetti, S., Cowan, C.E., Konneker, W.R. (1949), *Phys. Rev* **76**, 440.

DeBenedetti, S., Cowan, C.E., Konneker, W.R., Primakoff, H. (1950), *Phys. Rev.* **77**, 205-212.

Deutsch, M. (1951), *Phys. Rev.* **82**, 455-456.

Dirac, P.A.M. (1930), *Proc. Cambridge Philos. Soc.* **26**, 361-375.

Dugdale, S.B., Alam, M.A., Wilkinson, I., Hughes, R.J., Fisher, I.R., Canfield, P.C., Jarlborg, T., Santi, G. (1999), *Phys. Rev. Lett.* **83**, 4824-4827.

Egger, W., Kögel, G., Sperr, P., Triftshäuser, W., Rödling, S., Bär, J., Gudladt, H.-J. (2002), *Appl. Surf. Sci.* **194**, 214-217.

Foster, P.J., Mascher, P., Knights, A.P., Coleman, P.G. (2007), *J. Appl. Phys.* **101**, 043702-1-7.

Gidley, D.W., Köymen, A.R.,Capehart, T.W. (1982) *Phys. Rev. Lett.* **49**, 1779-1782.

Gidley, D.W. (1989), *Phys. Rev. Lett.* **62** 811-814.

Gidley, D.W., Frieze, W.E., Dull, T.L., Sun, J., Yee, A.F., Nguyen, C.V., Yoon, D.Y. (2000), *Appl. Phys. Lett.* **76**, 1282–1284.

Gilbert, S.J. Kurz, C., Greaves, R.G., Surko, C.M. (1997), *Appl. Phys. Lett.* **70**, 1944-1946.

Hirose, M., Nakajyo, T., Washio, M. (1997), *Appl. Surf. Sci.* **116**, 63-67.

Jeavons, A.P., Townsend, D.W., Ford, N.L., Kull, K., Manuel A.A., Fischer O., Peter, M. (1978), *IEEE Trans. Nucl. Sci.* **25**, 164-169.

Joliot-Curie, I., Joliot-Curie, F. (1934), *Nature* **133,** 201-202.

Kahana, S. (1963), *Phys. Rev.* **129**, 1622 – 1628.

Kawasuso, A., Okada, S. (1998), *Phys. Rev. Lett.* **81**, 2695-2698.

Landes, H.S., Berko, S., Zuchelli, A.J. (1956), *Phys. Rev.* **103**, 828-829.

Lock, D.G., Crisp, V.H.C., West, R.N. (1973), *J. Physics F* **3,** 561-570.

Lynn, K.G., Mills, A.P. Jr., West, R.N., Berko, S., Canter, K.F., Roellig, L.O. (1985), *Phys. Rev. Lett.* **54,** 1702-1705.

Lynn, K.G., MacDonald, J.R., Boie, R.A., Feldman, L.C., Gabbe, J.D., Robbins, M.F., Bonderup, E., Golovchenko, J. (1977), *Phys. Rev. Lett.* **38,** 241 – 244.

Mackenzie, I.K., Schulte, C.W., Jackman, T., Campbell, J.L. (1973), *Phys. Rev.* A **7**, 135-145.

Mader, J., Berko, S., Krakauer, H., Bansil, A. (1976), *Phys. Rev. Lett.* **37**, 1232-1236.

Maier, K., Peo, M., Saile, B., Scaefer, H.E., Seeger, A. (1979), *Phil. Mag. A* **40**, 701-728.

Mantl, S., Trifthäuser, W. (1978), *Phys. Rev. B* **17**, 1645-1652.

Mills, A.P. Jr. (1980), *Appl. Phys.* **22**, 273-276.

Mills, A.P.Jr., Platzman, P.M., Brown, B.L.(1978), *Phys. Rev. Lett.* **41**, 1076-1079.

Mogensen, O.E. (1974), *J. Chem. Phys.* **60**, 998-1004.

Mohorovičić, S. (1934), *Astron. nachr.* **14**, 93-108.

Mostafa, K.M., Caenegem, N.V., De Baerdemaeker, J., Segers, D., Houbaert, Y. (2007), *Phys. Stat. Sol.* **4**, 3554-3558.

Nagai, Y., Hasegawa, H., Tang, Z., Hempel, A., Yubuta, K., Shimamura, T., Kawazoe, Y, Kawai, A., Kano, F. (2000), *Phys. Rev. B.* **61**, 6574-6578.

Ociepa, J.G., Schultz, P.J., Griffiths, K., Norton, P.R. (1990), *Surf. Sci.* **225** 281-291.

Ohdaira, T., Suzuki, R., Mikado, T., Ohgaki, H., Chiwaki, M., Yamazaki, T. (1997), *Appl. Surf. Sci.* **116,** 177-180.

Ore, A. (1949), *Univ. Bergen Aarb. Naturvit. rekke* no. 9.

Ore, A., Powell, J.L. (1949), *Phys. Rev.* **75**, 1696 – 1699.

Osmon, P.E. (1965), *Phys. Rev.* **138**, B216-218.

Page, L.A., Heinberg, M. (1956), *Phys. Rev.* **102**, 1545 – 1553.

Petersen, K., Thrane, N., Cotterill, R.M.J. (1974), *Phil. Mag.* **29,** 9-23.

Roach, T., Bakshi, A., Canter, K.F. (1995) *Meas. Sci. Technol.* **6**, 496-501.

Rosenberg, I.J., Weiss, A.H., Canter, K.F. (1980), *Phys. Rev. Lett.* **44**, 1139-1142.

Ruark, A.E. (1945), *Phys. Rev.* **68**, 278.

Saarinen K., Laine, T., Kuisma, S., Nissila, J., Hautojarvi, P., Dobrzynski, L., Baranowski, J., Pakula, K., Stepniewski,R., Wojdak,M., Wysmolek,A., Suski,T., Leszczynski,M., Grzegory,I., Porowski, S. (1997) *Phys. Rev. Lett.* **79**, 3030 – 3033.

Stewart A.T. (1957), *Can. J. Phys.* **35,** 168-183.

Shearer, J.W., Deutsch, M. (1949), *Minutes of the Semi-Centennial Meeting at Cambridge,* in *Phys. Rev.* **76**, 462.

Shishido, I., Yasueda, H., Mizuno, M., Araki, H., Shirai, Y. (2007) *Phys. Stat. Sol*. C **4**, 3563-3566.

Siegle, A., Stoll, H., Castellaz, P., Major, J., Schneider, H., Seeger, A. (1997), *Appl. Surf. Sci.* **116**, 140-144.

Stepanov, S.V., Byakov, V.M. (2002), *J. Chem. Phys.* **116**, 6178-6195.

Triftshäuser, W., Kögel, G. (1982), Phys. Rev. Lett. 48, 1741-1744.

Van Veen, A., Schut, H., de Vries, J., Hakvoort, R.A., IJpma, M.R. (1990), *AIP Conf. Proc.* **218** (New York: AIP) 171-196.

Weber, M.H., Tang, S., Berko, S., Brown, B.L., Canter, K.F., Lynn, K.G., Mills, A.P., Roellig, L.O., Viescas, A.J. (1988), *Phys. Rev. Lett.* **61** 2542-2545.

Weber, M.H., Hunt, A.W., Golovchenko, J.A., Lynn, K.G. (1999), Phys. Rev. Lett. 83, 4658-4661.

Weisberg, H., Berko, S. (1967), *Phys. Rev.* **154**, 249-257.

Weiss, A.H., Mayer, R., Jibaly, M., Lei, C., Mehl, D., Lynn, K.G. (1988), *Phys. Rev. Lett.* **61**, 2245-2248.

West, R.N., Mayers, J., Walters, P.A. (1981), *J. Phys. E.* **14**, 478-488.

Wheeler, J.A., *Ann. New York Acad. Sci*. **48**, 219 (1946).

Zhu, J.G., Nadesalingam, M.P., Weiss, A.H., Tao, M. (2005), *J. Appl. Phys.* **97**, 103510-1-4.

Zitzewitz, P.W., Van House, J.C., Rich, A.,Gidley, D.W. (1979), *Phys. Rev. Lett*. **43**, 1281-1284.

Further Reading:

Charlton, M, Humberston, J.W. (2001), *Positron Physics*, Cambridge: Cambridge University Press.

Coleman, P.G. (Ed.) (2000), *Positron Beams and Their Applications*, Singapore: World Scientific.

Dupasquier, A., Mills, A.P. Jr. (Eds.) (1994), *Positron Spectroscopy of Solids, Proceedings of the International School of Physics "Enrico Fermi", Course LXXV*, Amsterdam: North Holland.

Gidley, D.W., Peng, H.-G., Vallery, R.S. (2006), *Ann. Rev. Materials Research* **36,** 49-79.

Jean, Y.C., Mallon, P.E., Schrader, D.M. (Eds.) (2003), *Positron and Positronium Chemistry*, Singapore: World Scientific.

Knights, A.P., Mascher, P., Simpson, P.J. (2007), *Proceedings of the 14th International Conference on Positron Annihilation, Phys. Stat. Sol.* **4**, 3413-4040.

Krause-Rehberg, R., Leipner, H.S. (1999), *Positron Annihilation in Semiconductors: Defect Studies*, Berlin: Springer.

Mills, A.P. Jr., Crane, W.S., Canter, K.F. (Eds.) (1986), *Positron Studies of Solids, Surfaces and Atoms*, Singapore: World Scientific.

Pethrick, R.A. (1997), *Prog. Polymer Sci.* **22**, 1-47.

Surko, C.M., Greaves, R.G., *Phys. Plasmas* **11**, 2333 (2004).

Weiss, A (1995), in *The Handbook of Surface Imaging and Visualisation,* ed. Hubbard, A.T. (CRC Press).

Figure captions

Figure 1. (left) Standard fast-fast analogue timing system: PM TUBE- photomultiplier tube/scintillator assembly: CF DIFF DISC - constant fraction differential discriminator: DELAY - ns delay box or cable: TAC - time-to-amplitude converter: MCA - multi-channel analyser. (right) Digital equivalent of an analogue timing system.

Figure 2. 2γ annihilation in (left) centre-of-mass frame and (right) laboratory frame

Figure 3. Schematic diagram of 2D ACAR apparatus. Positrons are guided from source to target by a strong (~1T) magnetic field. Courtesy Bristol positron group.

Figure 4. Basic set-up for Doppler broadening spectroscopy

Figure 5. Regions of interest defined for DBAR: sharpness parameter S = C/T, wing parameter W = (A+E)/T, where T = A+B+C+D+E.

Figure 6. 2D raw data from coincidence DBAR measurement. The peak, indicated by the diagonal from top left to bottom right, is $\sqrt{2}$ narrower than a single-detector spectrum, and has essentially no background. Courtesy Halle positron group.

Figure 7. Magnetic-transport positron beam system. A-grounded shield: B-standoff insulators: C-coils for magnetic field: D-source/moderator: E-*ExB* plates: F-lead shielding: G-accelerator: H-bellows: I= aperture: J-guiding coils: K=turbopump: L=sample manipulator: M= sample chamber: N=CEMA/CCD camera

Figure 8. Example of an electrostatic positron beam system. (a) source, (b) electrostatic reflector, (c) sample, (d) electrostatic lenses, (e) microchannelplate detector.

Figure 9. Reflection-geometry brightness enhancement stage. A,B – remoderator surfaces, C – target.

Figure 10. 10 μm square intensity cross-sectional image of a 5keV positron microbeam at Brandeis (Canter *et al.*, 1994). The central white peak area contains approx. 465 counts per pixel, and the ring marked with arrows contains about 180 counts per pixel. Reproduced by permission, AIP.

Figure. 11. Energy distribution of a pulse of positrons extracted from a thermalised room temperature positron plasma stored in a Penning trap [Gilbert et al, 1997]. Reproduced by permission, AIP.

Figure 12. Temperature dependence of the mean positron lifetime in Cu_3Sn. Error bars are within the points. Circles – ramping up, crosses – ramping down in temperature (Shishido *et al.*, 2007). Reproduced by permission, Wiley-VCH.

Figure 13. Normalized S(*E*) for FZ Si unimplanted and implanted with 2MeV Si^+ ions at doses of 10^n cm^{-2} (*n* = 11, 12, 13, 14 and 15) (Coleman *et al.*, 2002).

Figure 14. CDBAR ratios of $Fe_{0.99}Cu_{0.01}$ to pure Fe: (a) pure Cu, (b) alloy as quenched, the after ageing at 550ºC for (c) 0.1h, (d) 0.2h, (e) 2h, (f) 10h, (g) 100h, (h) 312 h (Nagai *et al.*, 2000). Reproduced by permission, APS: http://link.aps.org/abstract/PRB/v61/p6574.

Figure 15. W_o-W_i map for TiO2 stacks on SiC stacks and for SiC substrates. The 'pure state' points for SiC and TiO_2 are shown as circles, as are the two closely-related interface state (IS) (Coleman *et al.*, 2007).

Figure 16. (left): experimental (left) and calculated electron density of $LuNi_2B_2C$ projected along the [001] direction. Black signifies holes, white represents electrons. (right): Fermi surface topology of $LuNi_2B_2C$ – experimental (top) and theory for 3rd band in the (001) plane through the Γ point. The arrow indicates the nesting feature. From Dugdale *et al.* (1999). Reproduced by permission, APS: http://link.aps.org/abstract/PRL/v83/p4824.

Figure 17. The o-Ps lifetime τ_3, its intensity I_3, the e^+ lifetime τ_2, and the average positron lifetime τ_{av} in poly[$(EG)_{23}$DMA]; from Bamford *et al.* (2001). Reproduced by permission, AIP.

Figure 18. Void size distributions derived from Ps lifetime measurements in low-dielectric thin films of MSSQ. The solid and broken lines refer to cube- or channel-shaped pores. (Gidley *et al.*, 2000). Reproduced by permission, AIP.

Figure 19. PAES spectra for a Se-passivated Si(001) after isochronal annealing at increasing temperatures (Zhu *et al.*, 2005). Reproduced by permission, AIP.

Figure 20. Digital LEPD spot pattern from GaAs(110). The boxes indicate the regions used to evaluate signal intensity (Chen *et al.*, 1993). Reproduced by permission, APS: http://link.aps.org/abstract/PRB/v48/p2400.

Figure 21. Positron re-emission microscope image of Ni foil with contrast due to positron trapping at defects. Magnification 1150. Data collection time 14h., White areas have ~ 40 counts/pixel. From Brandes *et al.*, 1988. Reproduced by permission, APS: http://link.aps.org/abstract/PRL/v61/p492.

Figure 22. Positron lifetime image of a fatigue crack in copper taken by the Munich scanning positron microscope ; lifetimes range from 200 to 250 ps. Incident positron energy = 5keV. (David *et al.*, 2001). Reproduced by permission, Elsevier.

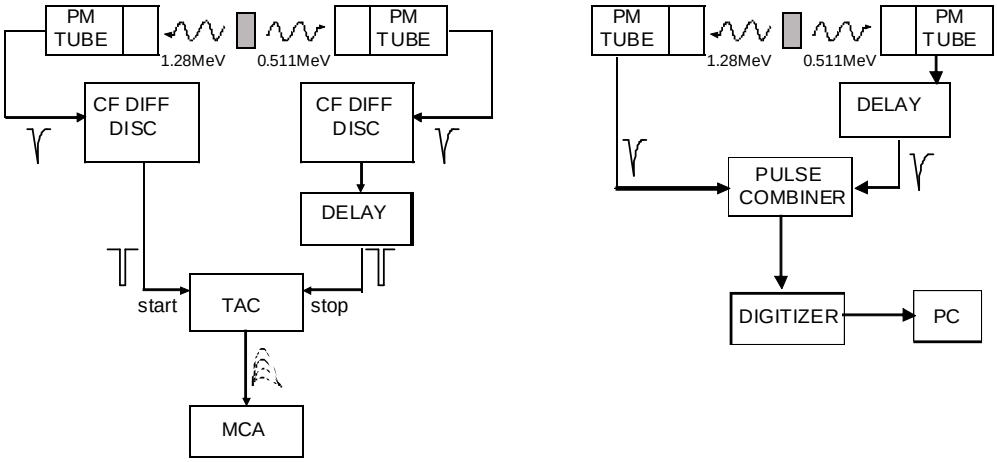
PM TUBE
1.28MeV
0.511MeV
PM TUBE
CF DIFF DISC
CF DIFF DISC
DELAY
start
TAC
stop
MCA
PM TUBE
1.28MeV
0.511MeV
PM TUBE
DELAY
PULSE COMBINER
DIGITIZER
PC

Figure 1

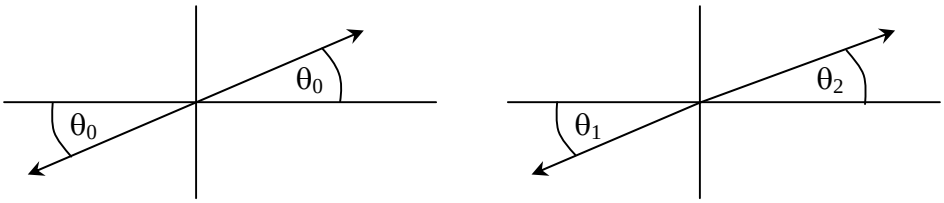

Figure 2.

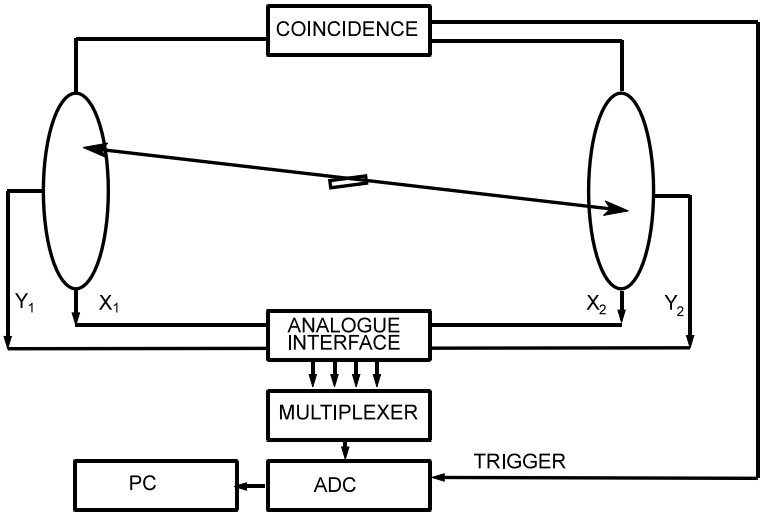
COINCIDENCE
Y1
X1
X2
Y2
ANALOGUE
INTERFACE
MULTIPLEXER
TRIGGER
PC
ADC

Figure 3.

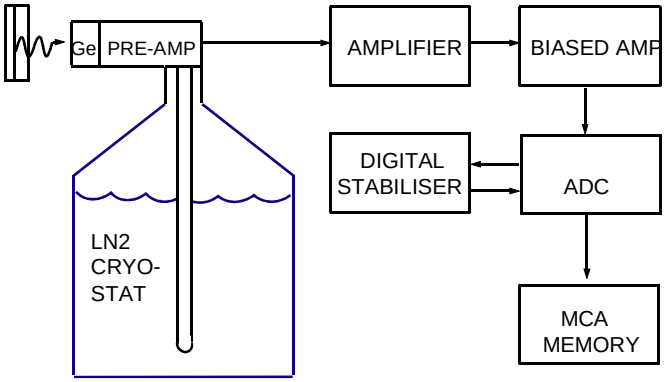
Ge
PRE-AMP
AMPLIFIER
BIASED AMP
DIGITAL
STABILISER
ADC
LN2
CRYO-
STAT
MCA
MEMORY

Figure 4

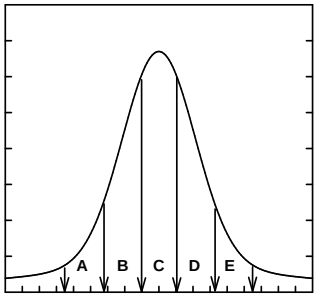

Figure 5.

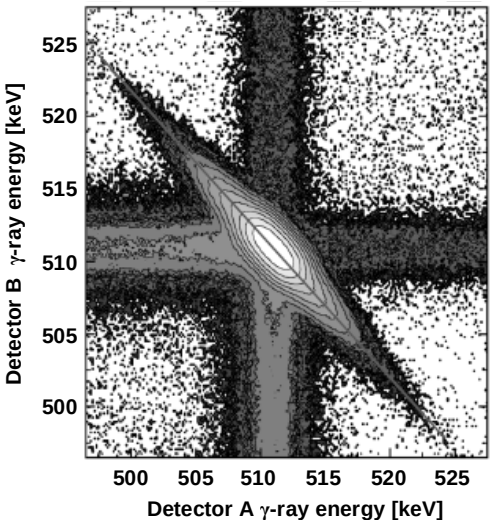
525
520
515
510
505
500
Detector B γ-ray energy [keV]
500 505 510 515 520 525
Detector A γ-ray energy [keV]

Figure 6.

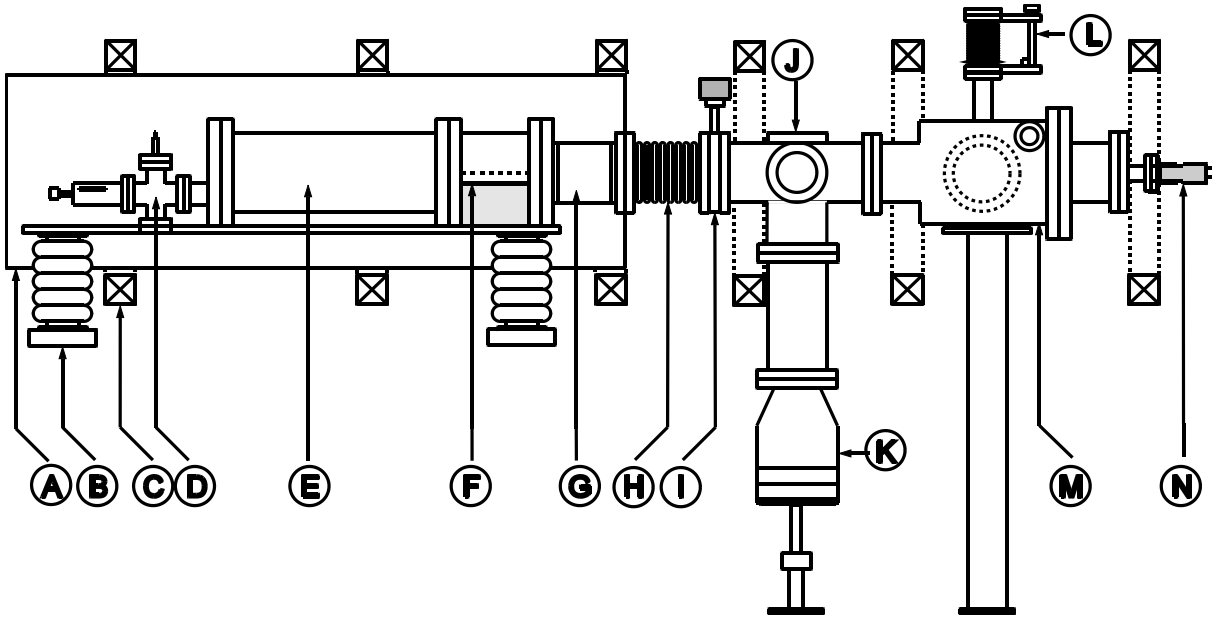

Figure 7.

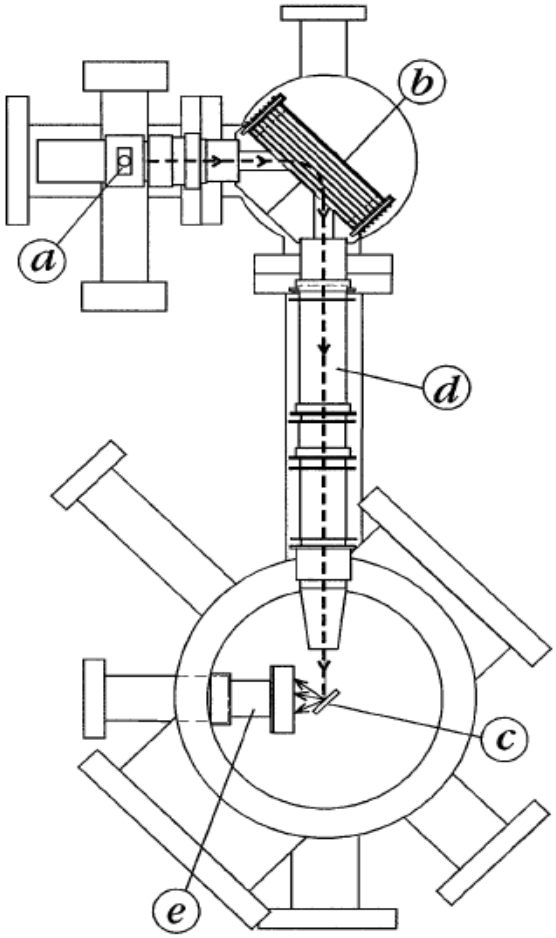

Figure 8.

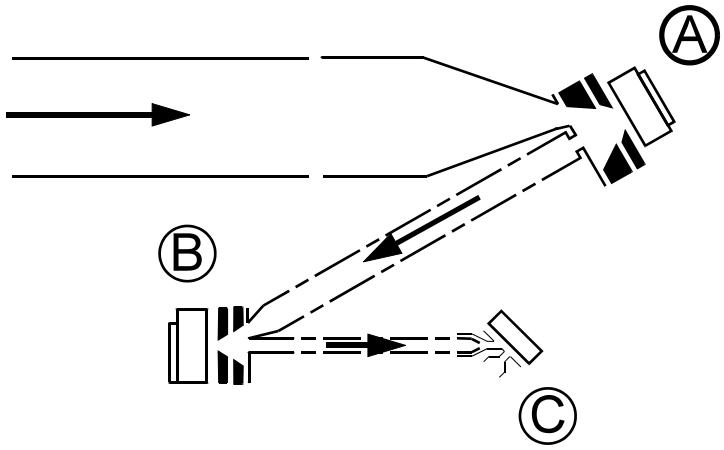

Figure 9

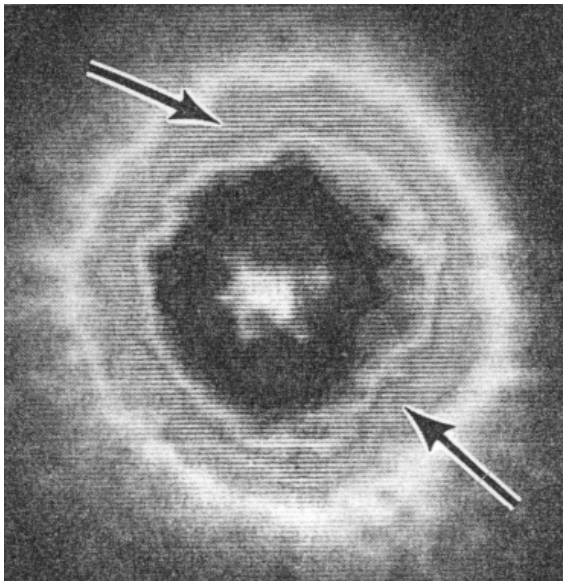

Figure 10.

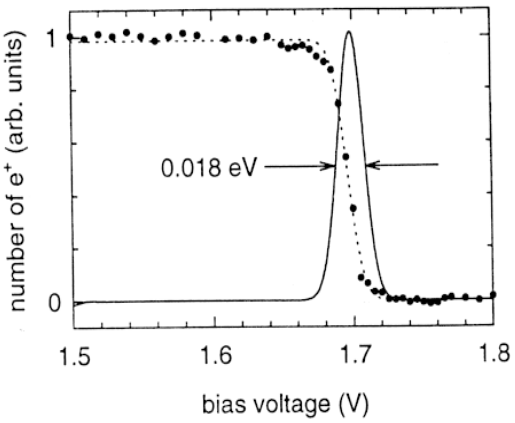

Figure. 11

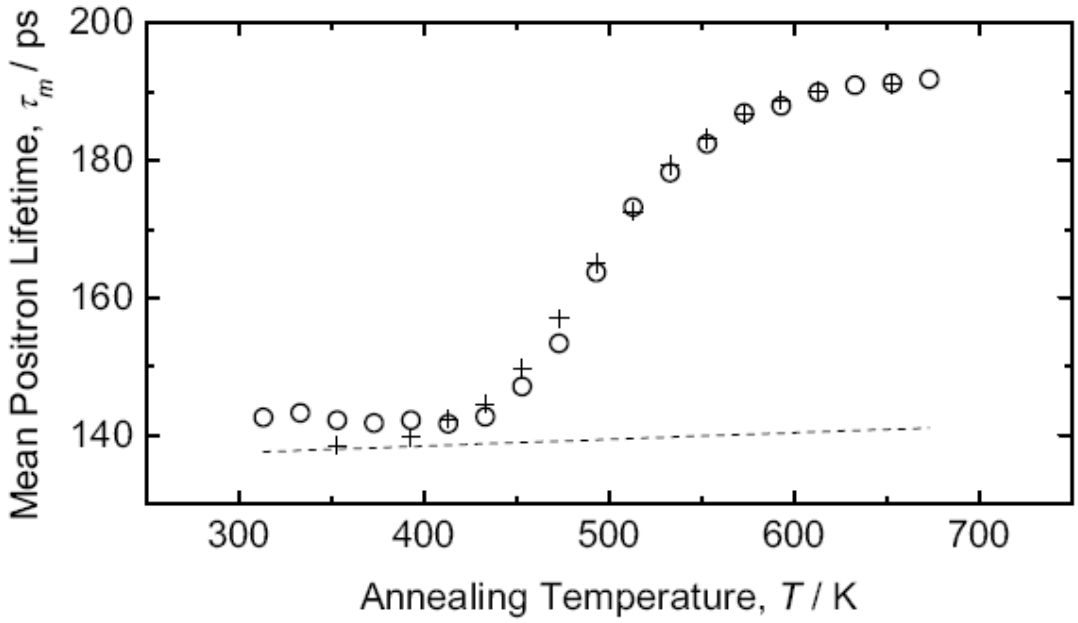
Mean Positron Lifetime, τ_m / ps
200
180
160
140
300
400
500
600
700
Annealing Temperature, T / K

Figure 12.

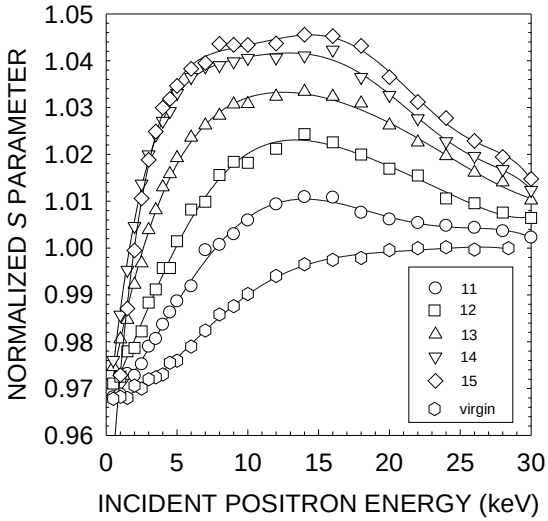
NORMALIZED S PARAMETER
1.05
1.04
1.03
1.02
1.01
1.00
0.99
0.98
0.97
0.96
0
5
10
15
20
25
30
INCIDENT POSITRON ENERGY (keV)
11
12
13
14
15
virgin

Figure 13.

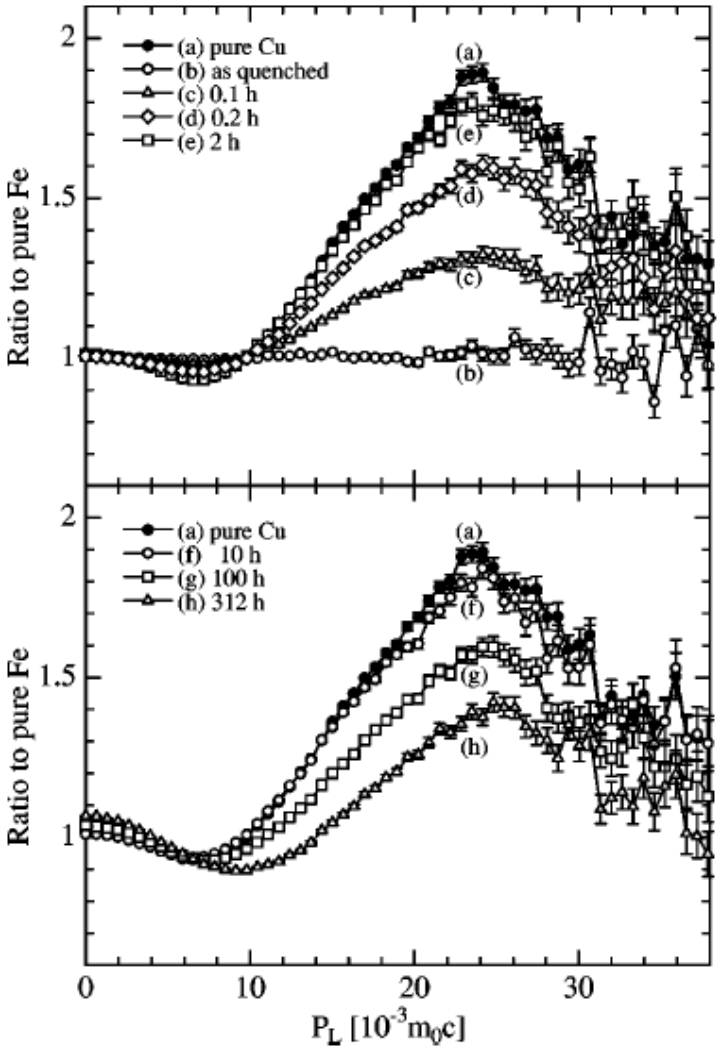
(a) pure Cu
(b) as quenched
(c) 0.1 h
(d) 0.2 h
(e) 2 h
(a) pure Cu
(f) 10 h
(g) 100 h
(h) 312 h
Ratio to pure Fe
Ratio to pure Fe
P_L [10^-3 m_0 c]

Figure 14.

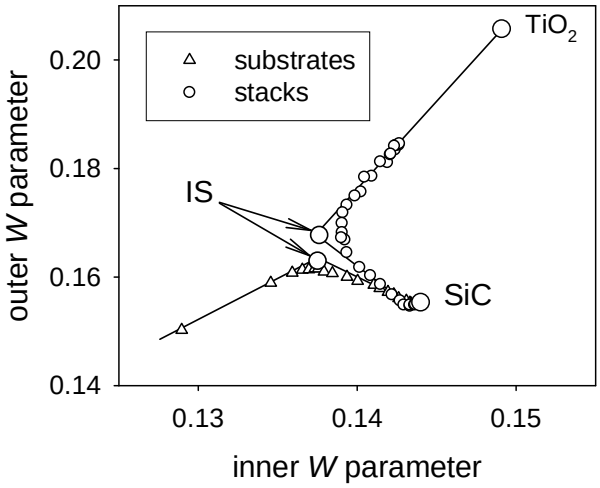
substrates
stacks
IS
TiO2
SiC
0.20
0.18
0.16
0.14
0.13
0.14
0.15
outer W parameter
inner W parameter

Figure 15.

Figure 16

.

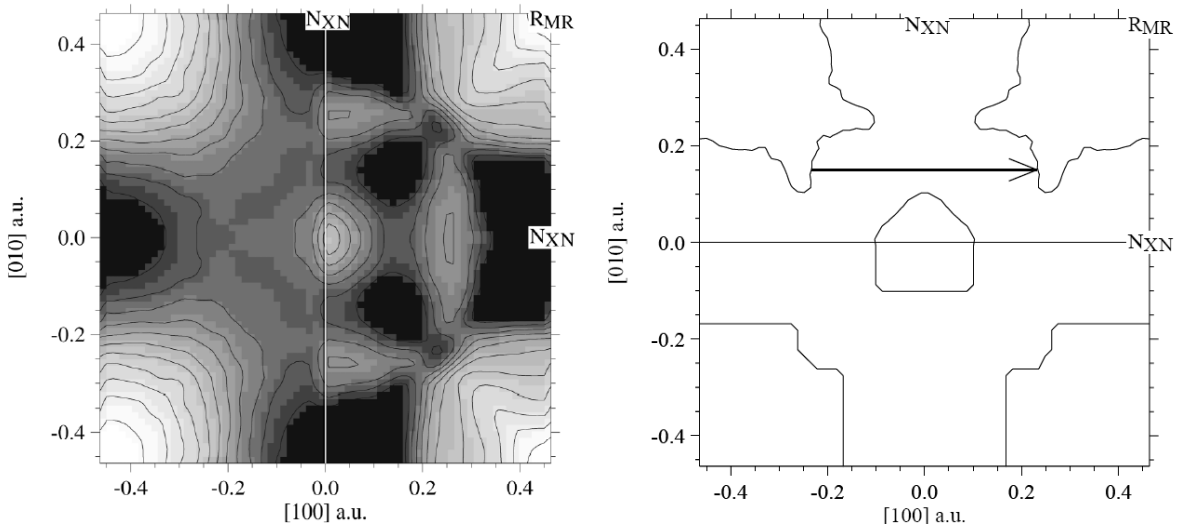
N_XN
R_MR
N_XN
[010] a.u.
[100] a.u.
0.4
0.2
0.0
-0.2
-0.4
-0.4
-0.2
0.0
0.2
0.4
N_XN
R_MR
N_XN
[010] a.u.
[100] a.u.

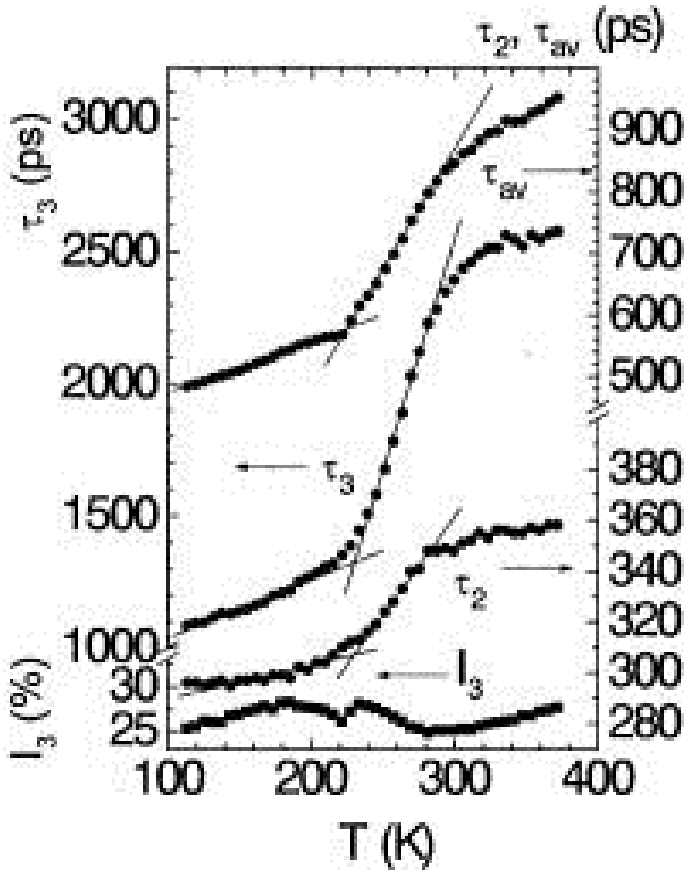
τ2, τav (ps)
τ3 (ps)
3000
2500
2000
1500
1000
900
800
700
600
500
380
360
340
320
300
280
τav
τ3
τ2
I3
I3 (%)
30
25
100
200
300
400
T (K)

Figure 17.

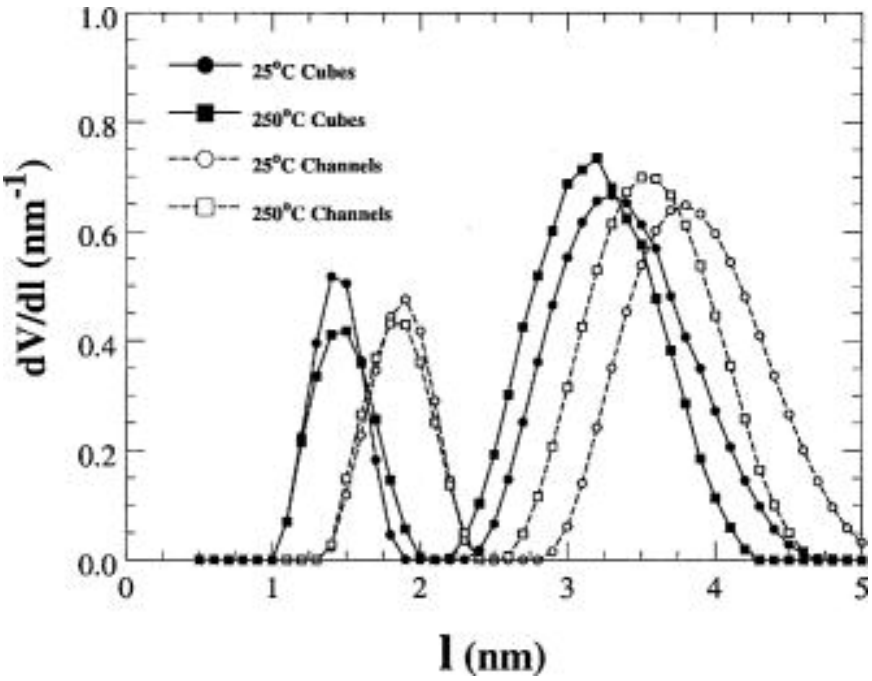
25°C Cubes
250°C Cubes
25°C Channels
250°C Channels
dV/dl (nm-1)
l (nm)
0.0
0.2
0.4
0.6
0.8
1.0
0
1
2
3
4
5

Figure 18.

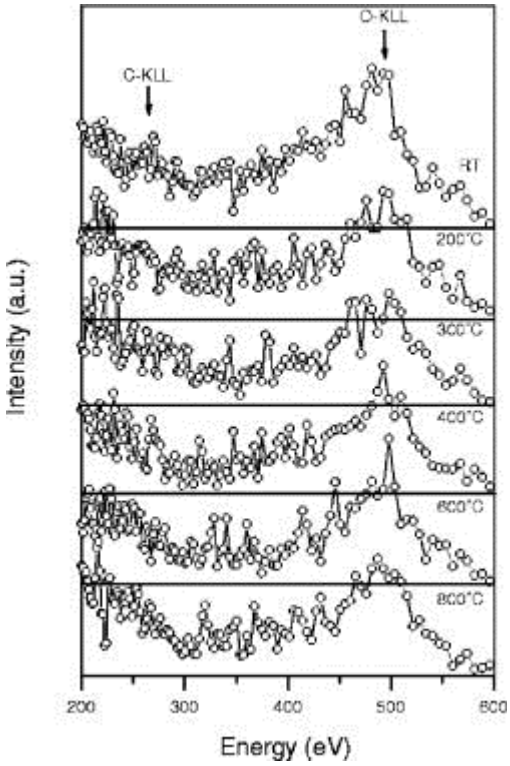
O-KLL
C-KLL
RT
200°C
300°C
400°C
600°C
800°C
Intensity (a.u.)
200
300
400
500
600
Energy (eV)

Figure 19.

Figure 20.

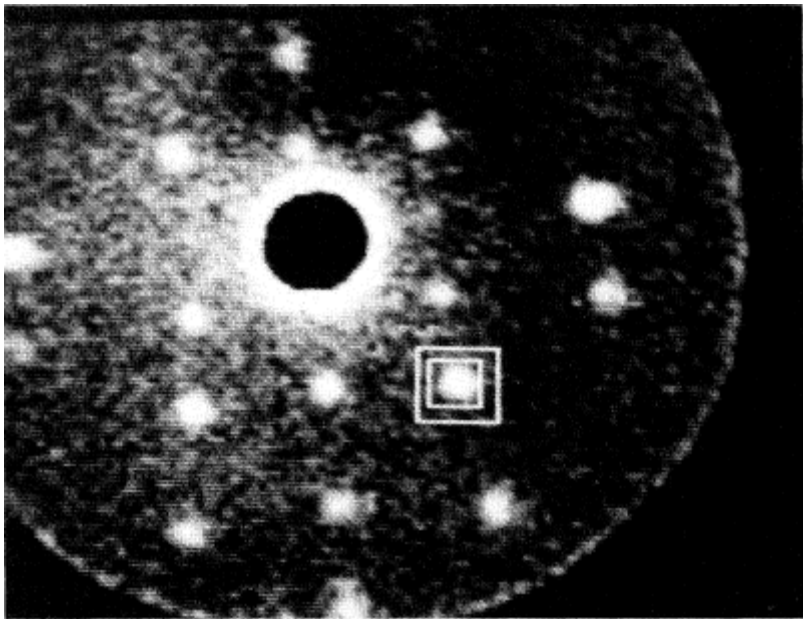

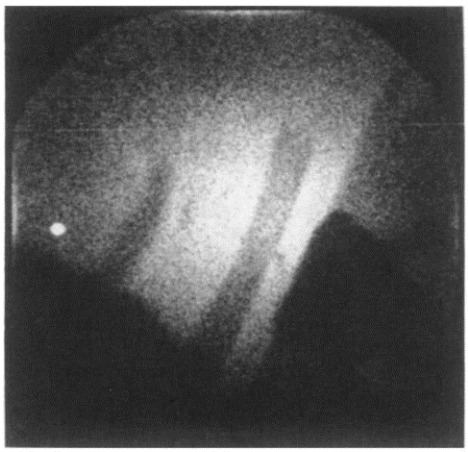

Figure 21

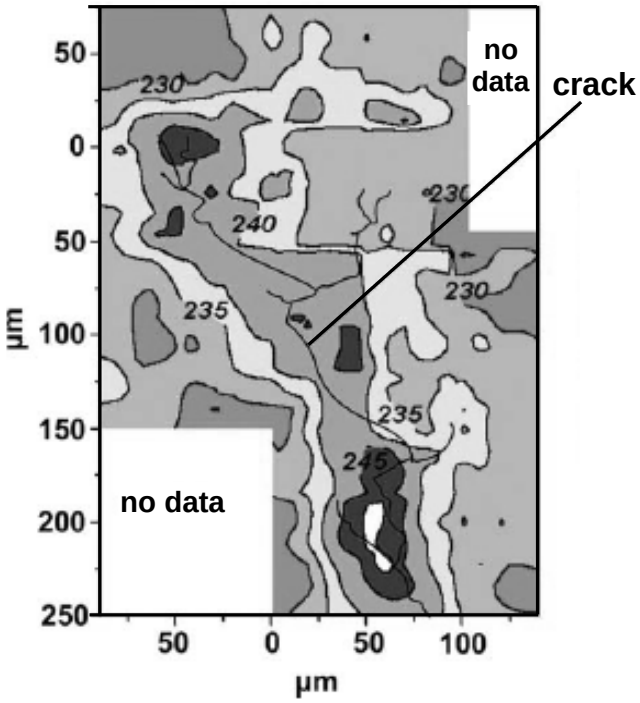
no
data
crack
230
240
230
230
235
235
245
no data
50
0
50
100
150
200
250
µm
50
0
50
100
µm

Figure 22.